AN ABSTRACT OF THE DISSERTATION OF

Ali Shahbaz Haider for the degree of Doctor of Philosophy in Electrical and Computer Engineering presented on September 01, 2021.

Title: Application of Nonlinear Model Predictive Controller for Ocean Wave Energy Conversion Systems.

Abstract approved:

_____

Ted K.A. Brekken

This work addresses the application of Nonlinear Model Predictive Control (NMPC) to a class of ocean wave energy conversion systems in which the cost functional is not in a standard quadratic form, and the WEC model includes the nonlinear effects, such as the hydrodynamic viscous drag. The NMPC implementation is extended for MIMO WEC problems. Hybrid testing of the proposed method is performed using Linear Testbed (LTB) wave simulator at Wallace Energy Systems and Renewables Facility (WESRF) at Oregon State University. Simulations and experiments are conducted to verify the proposed methodology.

Application of Nonlinear Model Predictive Controller for Ocean Wave Energy Conversion Systems

by
Ali Shahbaz Haider

A DISSERTATION

submitted to

Oregon State University

in partial fulfillment of
the requirements for the
degree of

Doctor of Philosophy

Presented September 01, 2021
Commencement June 2022

Doctor of Philosophy dissertation of Ali Shahbaz Haider presented on September 01, 2021

APPROVED:

Major Professor, representing Electrical and Computer Engineering

---

Head of the School of Electrical Engineering and Computer Science

---

Dean of the Graduate School

I understand that my dissertation will become part of the permanent collection of Oregon State University libraries. My signature below authorizes release of my dissertation to any reader upon request.

Ali Shahbaz Haider, Author

ACKNOWLEDGEMENTS

I want to thank my supervisor, Prof. Ted Brekken, for his guidance and support. I appreciate the help and support of Energy Systems' faculty members, Dr. Eduardo Cotilla-Sanchez and Dr. Yue Cao. It has been a great working experience with Dr. Bret Bosma and Alan McCall. Thanks to my colleges Jesse and Leila for their great company and David, Michael, Trenton, Derek, Michael, and Alastair for being very nice fellows. Lastly, thanks to the Fulbright commission for granting me a Fulbright scholarship for my PhD program.

CONTRIBUTION OF AUTHORS

I would like to thank Alan McCall from Dehlsen Associates, LLC, Santa Barbra, California, USA, who has been the industry partner in our work related to the CENTIPOD wave energy converter. It has been a great experience working with him.

TABLE OF CONTENTS

Page

TABLE OF CONTENTS (Continued)

Page

LIST OF FIGURES

Figure Page

LIST OF FIGURES (Continued)

Figure Page

LIST OF FIGURES (Continued)

Figure Page

LIST OF FIGURES (Continued)

Figure Page

LIST OF TABLES

Table Page

DEDICATION

To professor Ted Brekken who is always there for his students.

Application of Nonlinear Model Predictive Controller for Ocean Wave Energy Conversion Systems

1 General Introduction

1.1 Background and Motivation

Renewable energy technologies present a viable, sustainable solution to the growing energy demands of the world. The ocean provides the potential for an enormous untapped energy resource. Interest in ocean wave energy has triggered research in the optimal power capture techniques for wave energy converters. Achieving optimal power capture by a WEC is a multifaceted objective. It depends on factors such as the physical design of the WEC, the ocean conditions, and the control techniques. Model Predictive Control (MPC) is a promising control approach for wave energy converters' relatively slow plant dynamics because it maximizes energy capture while respecting the system's mechanical limits

The motivation for this work stems from a project at OSU in collaboration with partners from the ocean wave generation industry, namely, Dehlsen Associates, California, Wedge Global, Spain, McCleer Power, Michigan, and National Renewable Energy Lab (NREL), Colorado. This project involved testing and controlling the Power Take-Off (PTO) mechanism for the ocean Wave Energy Converter (WEC). The project milestones at OSU involved designing high-level MPC for the PTO machines from Wedge Global and McCleer Power, as shown in Figure 1-1. The experimental current-force characteristics of the PTO machines were highly nonlinear, and the resultant NMPC optimal control formulation was in a non-standard form, which would be discussed in detail in later chapters. The key motivation was implementing a real-time

Nonlinear MPC (NMPC) for these non-standard problem classes and extending the idea to Multiple-Input-Multiple-Output (MIMO) WEC systems. Moreover, the application of NMPC was expanded to include nonlinear time-varying parameter systems.

Lastly, hybrid testing of the proposed method is performed using Linear Testbed (LTB) wave simulator at Wallace Energy Systems and Renewables Facility (WESRF). Simulations and experiments are conducted to demonstrate the success of the proposed methodology.

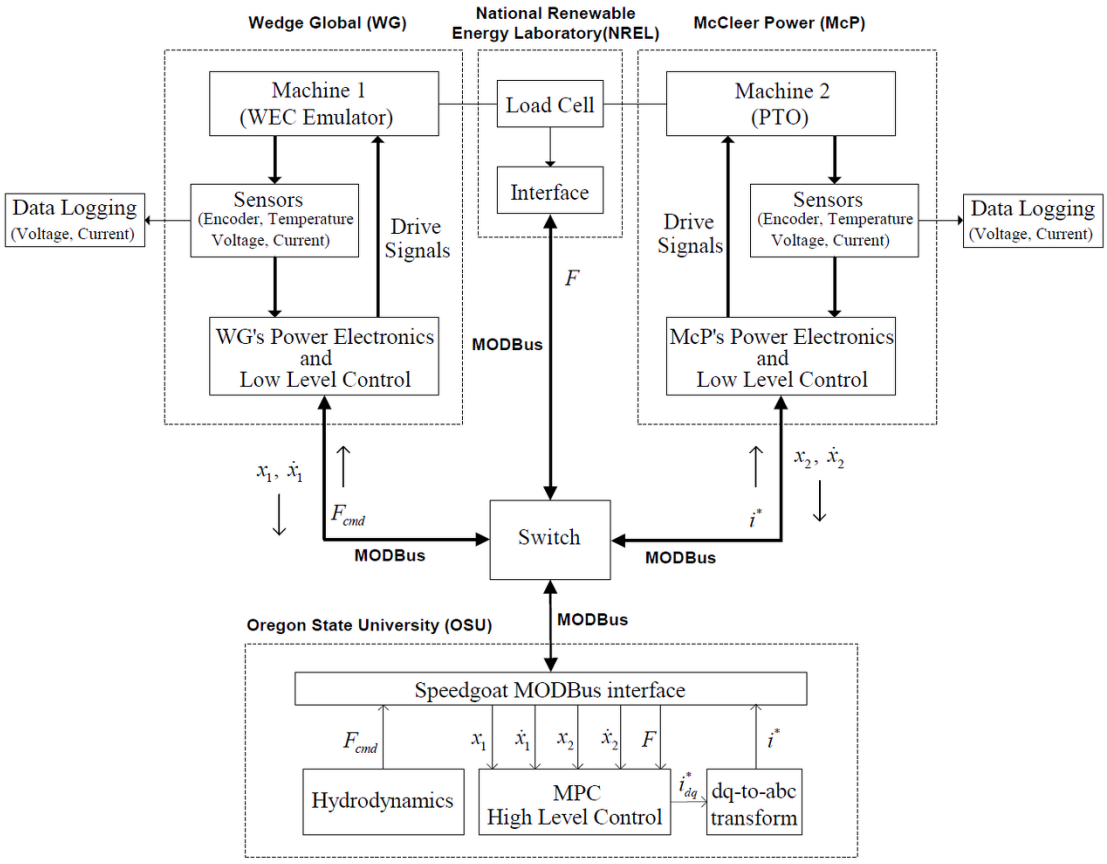

Figure 1-1 Layout of the MPC design project at OSU in collaboration with the industry partner.

1.2 The Layout of the Dissertation

This dissertation has been prepared in a manuscript style. The related work from three manuscripts has been presented chapter-wise, followed by a general conclusion section. A separate reference section is included for each chapter. The relevant manuscripts are included as appendixes at the end of this document.

2 Manuscript 1:

Application of Realtime Nonlinear Model Predictive Control for Wave Energy Conversion

Ali S. Haider, Ted K.A. Brekken, Alan McCall

IET Renewable Power Generation

IET USA Inc. 379, New Jersey, NJ 08837, USA

16 July 2021

2.1 Abstract

This article presents an approach to implement a Nonlinear Model Predictive Controller (NMPC) in real-time with a non-standard cost index. The proposed technique's applications are presented to maximize the energy produced by a Wave Energy Converter (WEC) when the cost index is a non-quadratic piecewise discontinuous functional of some design variables. The presented framework is based on pseudo-quadratization and weight scheduling, which is implemented using the ACADO toolkit for MATLAB/Simulink. The proposed strategy features code generation and deployment on the real-time target machines for industrial applications. The simulations and experiments confirm the success of the proposed approach in achieving the feasible operation of the NMPC and an optimal power capture by the wave energy converters.

2.2 Introduction

Renewable energy technologies present a viable, sustainable solution to the growing energy demands of the world. The ocean provides a potential for an enormous untapped energy resource [1]. Interest in ocean wave energy has triggered research in the optimal power capture techniques for wave energy converters. Achieving optimal power capture by a WEC is a multifaceted objective. It depends on factors such as the physical design of the WEC, the ocean conditions, and the control techniques. Model Predictive Control (MPC) is a promising control approach for wave energy converters' relatively slow plant dynamics because it maximizes energy capture while respecting the system's mechanical limits [2]. MPC is a look ahead control strategy that predicts future system behavior to solve a constrained optimization problem and determines the best control

action to maximize the output power of a WEC [3]. The MPC algorithm uses an internal model of the plant to predict the future states of the system. Most of the literature formulates the MPC problem by considering linear WEC plant dynamics with a quadratic performance index [4]. Nonlinear MPC design is required if nonlinear or time-varying plant dynamics are addressed, such as nonlinear mooring force and time-varying PTO dynamics [5]. However, most of the research on this subject focuses on formulating some form of standard convex quadratic performance functional for either a linear or nonlinear MPC optimization problem. The primary reason for such a formulation is the availability of efficient algorithms to solve standard convex optimization problems. The execution time becomes a significant concern when the ultimate objective is to solve the optimization problem and deploy the algorithm on real-time target machines to control the PTO mechanisms [6].

An increase in the WEC efficiency requires considering the nonlinear effects in the WEC dynamics and the PTO mechanisms and treating the whole system in an integrated way, i.e., the point absorber dynamics, the PTO system, and the control strategy. This results in MPC optimization formulations that have nonconvex and non-standard cost functionals. The capability of an NMPC formulation to handling such non-standard cost indexes is still mostly an unaddressed issue. This issue becomes important during the deployment phase of NMPC in real-time applications; for example, the NMPC designed in [5] does not focus on the real-time applicability of the proposed solution. Nonlinearities in the WEC dynamic models and non-standard cost functions are addressed using pseudo-spectral methods and differential flatness in [7, 8], where the developed nonlinear program is solved by the Sequential Quadratic

Programming (SQP) method using MATLAB routines fmincon and quadprog. The Economic Model Predictive Control (EMPC) method is presented in [9, 10], where the concept of a tracking cost function is presented, and the cost function reflects the economic objective of the system. Pseudo-spectral methods and EMPC techniques are promising solutions but are computationally intensive for nonlinear MIMO systems with non-standard optimization objectives, especially if the end objective is deploying the proposed algorithm to an embedded controller using the available Real-Time Iterative (RTI) solvers.

This research presents a framework to implement NMPC in real-time for multiple degrees of freedom wave energy converters formulated as general time-varying nonlinear dynamic systems. It also considers the problems in which the PTO mechanisms' cost index takes non-standard forms, such as affine form, polynomial with a degree higher than two, piecewise polynomial of PTO force, trigonometric polynomials of design variables, and time-varying parametric. This work focuses on practical implementation considerations rather than in-depth mathematical formulation or algorithm design, for instance, the reformulation of a given non-standard NMPC problem for implementation on a real-time target-machine using a nonlinear optimization solver, such as ACADO, which supports differential-algebraic process dynamics and constraints [11, 12]. This paper explores the pseudo-quadratization technique to reformulate the non-quadratic objection functional to quadratic-like forms. This technique enables the use of available software package for the problem sets that have non-standard cost indexes.

Moreover, the technique of weight scheduling is presented to broaden the application of the proposed technique further to include the problems that require the optimization of cost indexes defined in a piecewise polynomial form. Such systems are common in the wave energy generation sector. The proposed method is applied to case study NMPC optimal power take-off (PTO) problems that take the form of a real-time optimization problem over a non-standard piecewise polynomial cost index.

2.3 Mathematical Formulation for NMPC

A given NMPC problem optimizes a manipulated variable u ⊆ w to maximize some cost functional P of a set of design variables w, while respecting the given system constraints. This research focuses on a class of NMPC problems in which the cost functional takes on a general nonlinear piecewise polynomial form. Considering the case of finite-horizon optimization, we can mathematically describe the NMPC problem of such a class as,

$$\max_{\mathbf{u}} \mathbf{P}(\mathbf{w}) = \begin{cases} P_1(\mathbf{w}) + \rho_{N,1}(\mathbf{w}) & w_n < R_1 \\ P_2(\mathbf{w}) + \rho_{N,2}(\mathbf{w}) & R_1 \le w_n \le R_2 \\ \vdots & \vdots \\ P_j(\mathbf{w}) + \rho_{N,j}(\mathbf{w}) & R_{j-1} \le w_n \le R_j \end{cases} \tag{1}$$

subject to,

$$\dot{\mathbf{x}} = \mathbf{g}(\mathbf{w}) \tag{2}$$

$$\mathbf{q} = \mathbf{p}(\mathbf{w}) \tag{3}$$

$$\boldsymbol{\Upsilon}_\mathbf{1} = \mathbf{B}_{\mathbf{equal}} \tag{4}$$

$$\mathbf{B}_{\mathbf{lower}} \le \boldsymbol{\Upsilon}_\mathbf{2} \le \mathbf{B}_{\mathbf{upper}} \tag{5}$$

where Υ_i vectors are of the following forms,

$$\begin{aligned} \boldsymbol{\Upsilon}_\mathbf{1} &= \boldsymbol{\Psi}_\mathbf{1}\mathbf{q}, \\ \boldsymbol{\Upsilon}_\mathbf{2} &= \boldsymbol{\Psi}_\mathbf{2}\mathbf{q} \end{aligned} \tag{6}$$

here, $\mathbf{g}$ and $\mathbf{p}$ are vectors of real-valued nonlinear functions of some design variables $\mathbf{w}$, and P_i and $\rho_{N,j}$ are real-valued polynomial functions of $\mathbf{w}$. The real-valued design variable $w_n \in \mathbf{w}$ is responsible for the switching of the cost manifold in (1) depending upon its magnitude lying in a particular interval defined by some real numbers R_i. The description of various variables and constants in (1) through (6) is given in Table 2-1. The maximization of the cost functional in (1) is subjected to the dynamic constraints in (2), which corresponds to a general nonlinear state-space description of the physical WEC plant. The proposed NMPC formulation considers the nonlinear algebraic constraints described by (3). The equality and inequality constraints are described by (4) and (5), respectively. These constraints are formulated in (6) in terms of the algebraic expressions of the design variables.

Table 2-1 Notations

Variable	Description
$\mathbf{w}$	Set of design variables
N	Prediction horizon
$\mathbf{x} \subseteq \mathbf{w}$	State vector
$\mathbf{u} \subseteq \mathbf{w}$	Manipulated variable
$\rho_{N,i}$	Finite horizon terminal cost penalty
P_i	Real-valued polynomial of design variables
$\mathbf{\Psi_i}$	Constant matrices
$\mathbf{B_i}$	Constant column vectors
$\mathbf{\Upsilon_i}$	Column vectors of real-valued nonlinear functions
$\mathbf{q}$	Column vectors of real-valued nonlinear functions
R_i	Some real number
v_{pto}	Float heave velocity (m/s)
z_{pto}	Float heave position (m)
F_r	Radiation force (N)
F	Time integral of the radiation force
u	Control input, $F_{pto}(N)$
m	Float mass (kg)
A	Float added mass (kg)
k	Float hydrostatic stiffness (N/m)
c_i	Constants with $i, j \in \{a, b\}$
d	Excitation force disturbance, F_e (N)
I_{pto}	PTO generator current
M	Effective mass $m + A(\infty)$ (Kg)
$\mathbf{h}$	Column vectors of real-valued nonlinear functions
$\mathbf{h_N}$	Column vectors of real-valued nonlinear functions

2.4 Time Domain Model of a WEC

Consider a single degree of freedom heaving point absorber WEC with a linear generator PTO mechanism, as shown in Figure 2-1, a single input multiple output system with heave PTO force as the control input and the velocity and positions of the float as outputs. The time-domain model of a WEC with frequency-dependent damping has been developed and validated in [13, 14],

$$\mathbf{x} = [v_{pto} \quad z_{pto} \quad F_r \quad F]^T$$
$$\mathbf{g} = \begin{bmatrix} \frac{-k}{M} z_{pto} + \frac{1}{M} F_r + \frac{1}{M} u + \frac{1}{M} d \\ v_{pto} \\ -c_a v_{pto} - c_b z_{pto} - c_d F_r - c_e F \\ F_r \end{bmatrix} \tag{7}$$

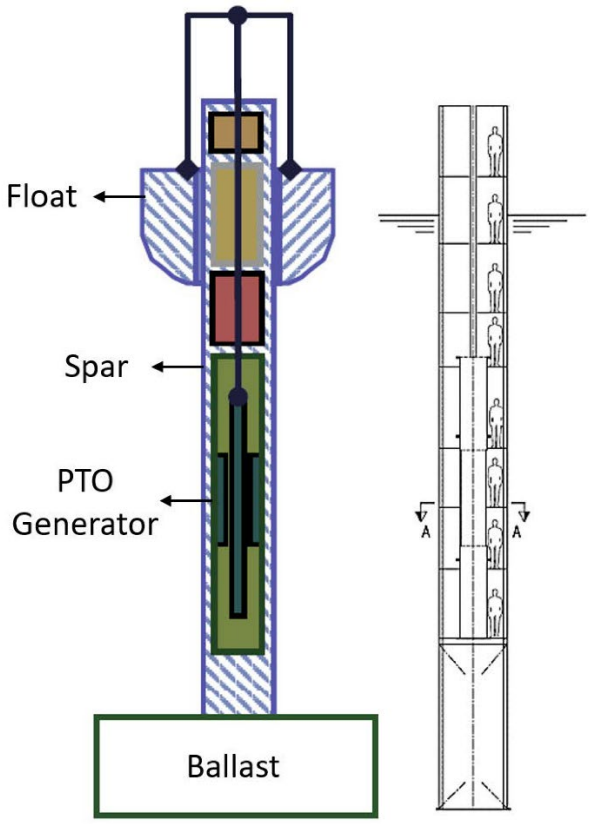

Figure 2-1 Point absorber WEC with linear generator PTO mechanism by Wedge-Global.

The description of various variables and constants in (7) is given in Table 2-1. The state-space form of the WEC dynamics in (7) becomes the differential constraints in (2). The dynamic system (7) may include time-dependent variables to incorporates some practical scenarios, such as a change in the configuration of float [14] or actively varying the number of PTO generator pickup coils.

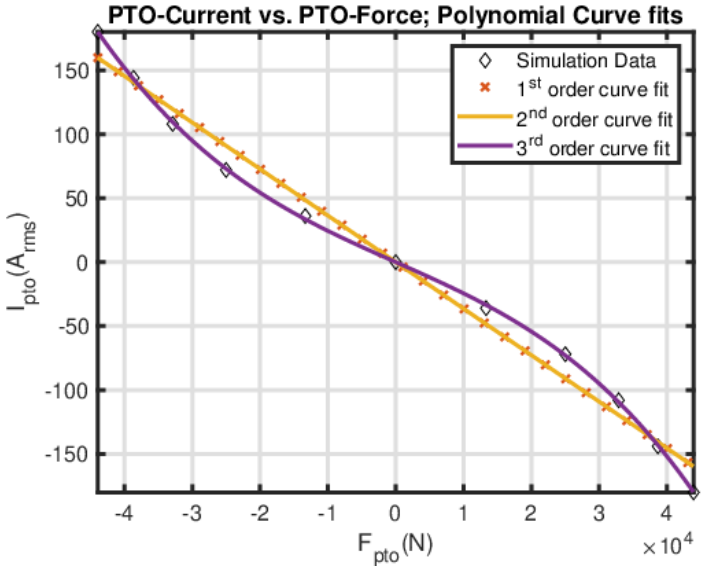

Figure 2-2 Higher-order current-force relation for a WEC PTO generator.

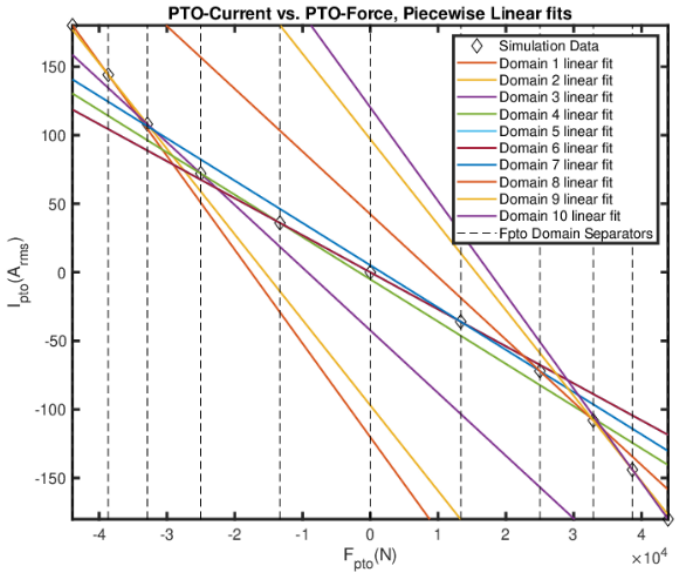

Figure 2-3 Piecewise linear current-force relation for a WEC PTO generator.

2.4.1 Nonquadratic WEC-PTO Models

The electrical power output from the PTO mechanism of the WEC is the difference between the mechanical power input from the waves and the losses in the PTO system. For a given PTO generator with a converter efficiency η_{Conv}, the copper loss constant K_{Cu}, and the winding resistance R_{Ω}, the electrical power cost functional to be maximized, including the electrical losses, is given by,

$$\max_{F_{pto}} P_E = \eta_{Conv}\left(F_{pto}v_{pto} - K_{Cu}I_{pto}^2 R_{\Omega}\right) \tag{8}$$

2.4.1.1 Higher-Order PTO Models

This case study scenario is taken from McCleer Power's Linear PTO generator with the PTO force-current characteristics given by Figure 2-2. This relation is described by a third-order curve fit between the PTO current and the PTO force,

$$I_{pto}\left(F_{pto}\right) = a_3 {F_{pto}}^3 + a_2 {F_{pto}}^2 + a_1 F_{pto} + a_0 \tag{9}$$

Putting (9) in (8), we get,

$$\begin{aligned} P_E = c_0 F_{pto} v_{pto} - (c_1 F_{pto}^6 + c_2 F_{pto}^5 + c_3 F_{pto}^4 \\ + c_4 F_{pto}^3 + c_5 F_{pto}^2 + c_6 F_{pto} + c_7) \end{aligned} \tag{10}$$

It can be seen that (10) is a higher-order non-quadratic cost functional to be maximized.

2.4.1.2 Piecewise Linear PTO Models

This case study scenario considers the data from Figure 2-2. However, the relation between the PTO current and the PTO force is approximated by the piecewise linear curves that fit between each of the two consecutive data points in Figure 2-3. Each

linear curve fit is valid for the corresponding domain of the PTO force. For Figure 2-3, these piecewise linear curve fits are described by (11).

$$I_{pto}(F_{pto}) = \begin{cases} a_{11}F_{pto} + a_{10} & F_{k1} \le F_{pto} < F_{k2} \\ a_{21}F_{pto} + a_{20} & F_{k2} \le F_{pto} < F_{k3} \\ a_{31}F_{pto} + a_{30} & F_{k3} \le F_{pto} < F_{k4} \\ \vdots & \vdots \\ a_{101}F_{pto} + a_{100} & F_{k10} \le F_{pto} < F_{k11} \end{cases} \tag{11}$$

Putting (11) in (8), we get,

$$P_{E,i} = c_0 F_{pto} v_{pto} - \left(c_{i1}F_{pto}^2 + c_{i2}F_{pto} + c_{i3}\right), \quad i \in \{1,2 \dots 10\} \tag{12}$$

It can be seen that (12) is a piecewise quadratic cost functional to be maximized. Comparing (8) with (12), we can observe that the power loss component of P_E in (12) is dependent upon the magnitude of PTO force. Each component represents a manifold, which is a 2-D surface, as shown by Figure 2-4.

2.4.1.3 Piecewise Nonlinear PTO Models

This case study scenario is taken from Wedge Global's linear PTO generator with the PTO force-current characteristics given by Figure 2-5. This relation is approximated by piecewise nonlinear curve fits over the PTO force domains. For Figure 2-5, these piecewise curve fits are described by (13).

$$I_{pto}(F_{pto}) = \begin{cases} \dfrac{F_{pto} - \alpha}{\beta} & F_{pto} \le -F_k \\ -\sqrt{\dfrac{-F_{pto}}{\gamma}} & -F_k < F_{pto} < 0 \\ \sqrt{\dfrac{F_{pto}}{\gamma}} & 0 \le F_{pto} < F_k \\ \dfrac{F_{pto} + \alpha}{\beta} & F_{pto} \ge F_k \end{cases} \tag{13}$$

Putting (13) in (8), we get (14).

$$P_E = \begin{cases} c_{10}F_{pto}v_{pto} + c_{11}F_{pto}^2 v_{pto} - c_{12}F_{pto}^2 + c_{13}F_{pto} + c_{14}v_{pto} - c_{15} & F_{pto} \le -F_k \\ c_{20}F_{pto}v_{pto} + c_{21}F_{pto} & -F_k < F_{pto} < 0 \\ c_{30}F_{pto}v_{pto} - c_{21}F_{pto} & 0 \le F_{pto} < F_k \\ c_{40}F_{pto}v_{pto} + c_{11}F_{pto}^2 v_{pto} - c_{12}F_{pto}^2 - c_{13}F_{pto} + c_{14}v_{pto} - c_{15} & F_{pto} \ge F_k \end{cases} \quad (14)$$

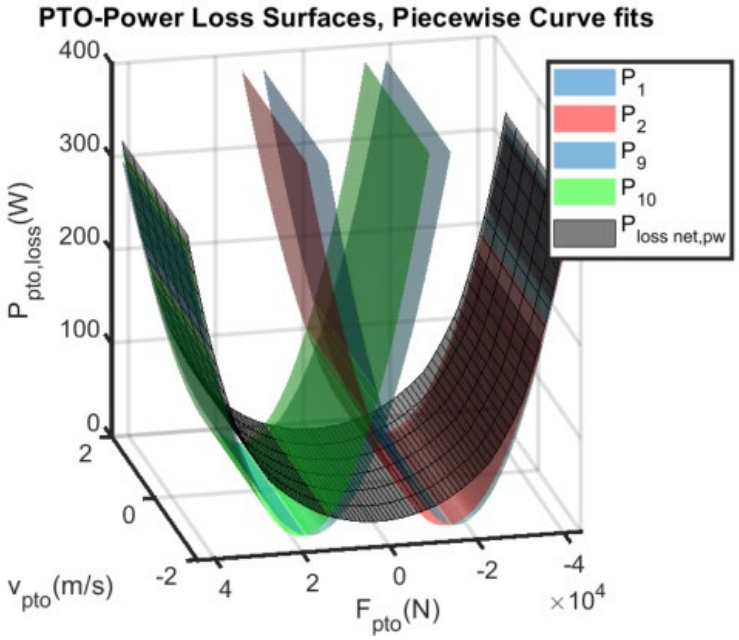

Figure 2-4 WEC-PTO power loss manifolds for piecewise linear curve fitting (only a few surfaces are shown for clarity).

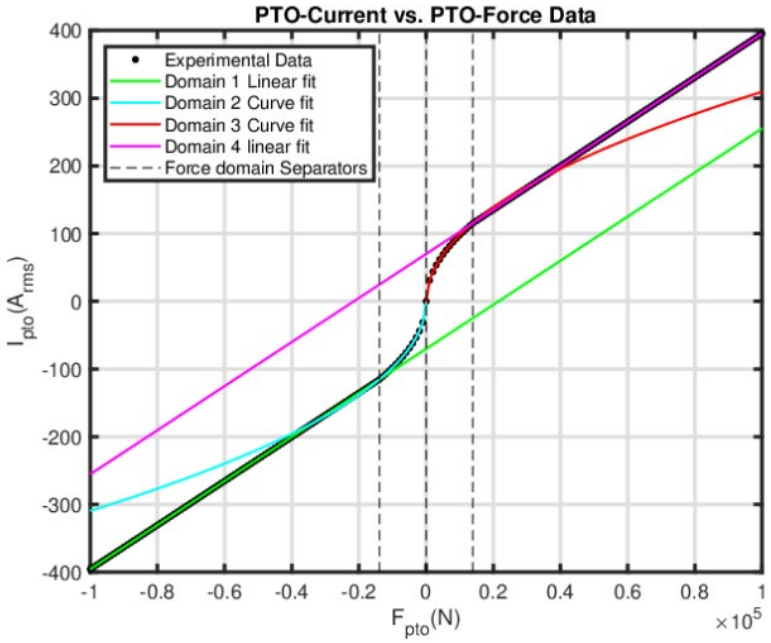

Figure 2-5 Piecewise nonlinear current-force relation for a WEC PTO generator.

It can be seen that (14) is a higher-order piecewise non-quadratic cost functional to be maximized. Comparing (14) with (8), we can observe that the power loss component of P_E in (14) is dependent upon the magnitude of PTO force. Each component represents a manifold, which is a 2-D surface, similar to Figure 2-4.

2.5 NMPC Implementation Method

The cost functionals in (10), (12), and (14) are not standard quadratic forms. To implement such problems, we have used the method of *pseudo-quadratization* and weight scheduling. With this technique, we can extend the capabilities of the standard quadratic solvers [11] to implement the NMPC for the non-standard optimization problems according to the scheme shown in Figure 2-6.

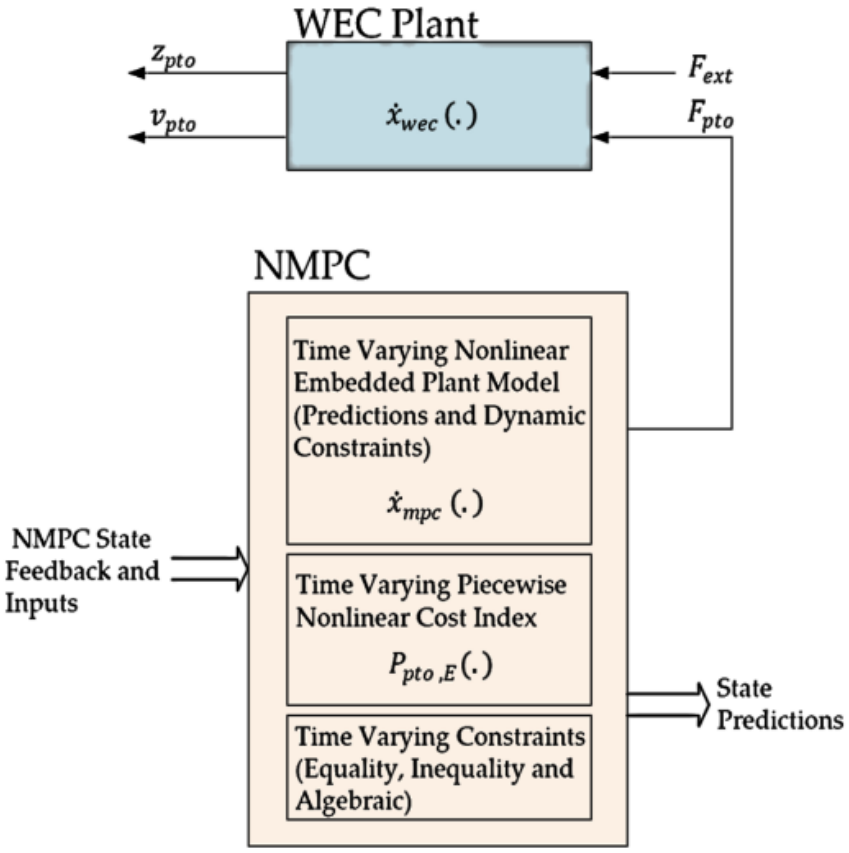

Figure 2-6 Implementing nonlinear MPC with ACADO Toolkit.

2.5.1 Pseudo-Quadratization and Weight Scheduling

If the cost functional P in (1) is not quadratic, then the technique of pseudo-quadratization relies on appropriately defining two vectors of nonlinear real-valued functions, $\boldsymbol{h}(\mathbf{w})$ and $\boldsymbol{h}_N(\mathbf{w})$ to convert P into quadratic-like forms. A proper selection of these vectors along with the weighting matrices W_i would enable us to put (1) into a form given by (15).

$$\begin{aligned} P_i(\mathbf{w}) &= \frac{1}{2}\mathbf{h}^{\mathbf{T}} W_i \mathbf{h}, \qquad i = 1,2 \dots, j \\ \rho_{N,i}(\mathbf{w}) &= \frac{1}{2}\mathbf{h}_{\mathbf{N}}^{\mathbf{T}} W_{N,i} \mathbf{h}_{\mathrm{N}}, \quad i = 1,2 \dots, j \end{aligned} \tag{15}$$

The expression in (15) resembles a quadratic form but might not expand to a quadratic polynomial of design variables, as we will discuss shortly; hence, they are named pseudo-quadratic forms. For nonconvex problems, the convex relaxation of the cost manifold P_i in (15) can be implemented by the superposition of some convexifying manifold D_i. Let us denote the modified manifold as $P_{i,m}$ and we can write it as,

$$P_{i,m}(\mathbf{w}) = \frac{1}{2}\mathbf{h}^{\mathbf{T}} W_i \mathbf{h} + D_i(\mathbf{w}) \tag{16}$$

The manifold D_i can be decomposed into the quadratic form using appropriate weighting matrices $W_{d,i}$,

$$D_i(\mathbf{w}) = \frac{1}{2}\mathbf{h}^{\mathbf{T}} W_{d,i} \mathbf{h} \tag{17}$$

Using (17) in (16), the modified manifold $P_{i,m}$ can be expressed as

$$P_{i,m}(\mathbf{w}) = \frac{1}{2}\mathbf{h}^{\mathbf{T}} \big(W_i + W_{d,i}\big)\mathbf{h} = \frac{1}{2}\mathbf{h}^{\mathbf{T}} W_{i,m} \mathbf{h} \tag{18}$$

The choice of D_i and hence, the weighting matrices $W_{d,i}$ are not unique and depend upon a specific cost functional (15) for a given problem. The manifold D_i can

be used to appropriately increase the weights of the convex terms of P_i in (15), for example F_{pto}^n, where n is an even number. Some other deciding factors are the convergence rate of the optimization algorithm and the modified cost manifold's allowed deviation in (18) from the actual cost manifold (1).

Now let us apply the above technique to the higher-order PTO model in (10). Defining a **h** vector as

$$\mathbf{h} = \begin{bmatrix} F_{pto}^3 & F_{pto}^2 & F_{pto} & v_{pto} & 1 \end{bmatrix}^T \tag{19}$$

Although (10) is not a quadratic form but using (20) in (10), we get a pseudo-quadratic form described by (21).

$$P_E = \frac{1}{2}\mathbf{h}^{\mathbf{T}} \left(2 \begin{bmatrix} -c_1 & \frac{-c_2}{2} & 0 & 0 & 0 \\ \frac{-c_2}{2} & -c_3 & \frac{-c_4}{2} & 0 & 0 \\ 0 & \frac{-c_4}{2} & -c_5 & \frac{c_0}{2} & \frac{-c_6}{2} \\ 0 & 0 & \frac{c_0}{2} & 0 & 0 \\ 0 & 0 & \frac{-c_6}{2} & 0 & -c_7 \end{bmatrix} \right) \mathbf{h} \tag{20}$$

The cost functional expression in (21) can be implemented using nonlinear optimization solver ACADO. Similarly, defining a vector **h** for (12) as,

$$\mathbf{h} = \begin{bmatrix} F_{pto} & v_{pto} & 1 \end{bmatrix} \tag{21}$$

Using (22) in (12), we get a weight-scheduled quadratic form described by (23).

$$P_{E,i} = \frac{1}{2}\mathbf{h}^{\mathbf{T}} \left(2 \begin{bmatrix} -c_{i1} & \frac{c_0}{2} & \frac{-c_{i2}}{2} \\ \frac{c_0}{2} & 0 & 0 \\ \frac{-c_{i2}}{2} & 0 & -c_{i3} \end{bmatrix} \right) \mathbf{h} \tag{22}$$

he cost functional expression in (23) can be implemented using nonlinear optimization solver ACADO using weight scheduling for the PTO force.

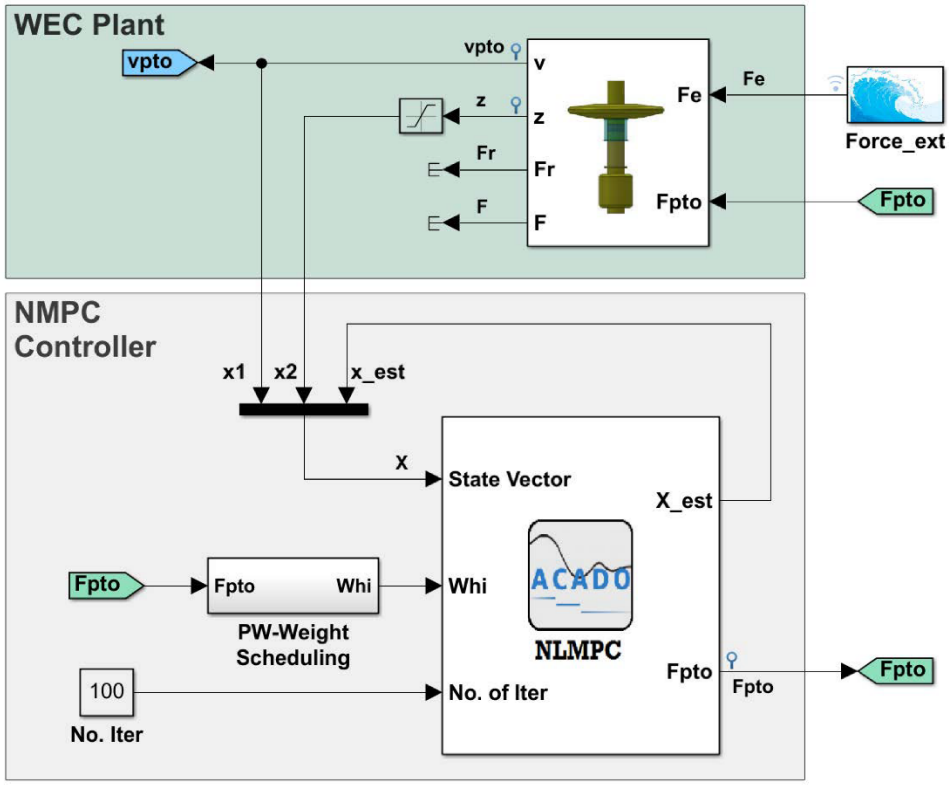

Figure 2-7 NMPC implementation in Simulink using ACADO Toolkit.

2.6 Simulation, Testing, and Results

The Simulink block diagram for the implementation of NMPC is shown in Figure 2-7 for the WEC in (7) using parameter values from [13] and the cost functional in (21). The test excitation force profile is shown in Figure 2-8, corresponding to a JONSWAP spectrum (significant wave height of 2.5 m, and peak period of 8 sec). The plots for the instantaneous PTO power and the average PTO power are shown in Figure 2-9. The NMPC optimization solution is convergent, and the locus of the PTO force and the PTO velocity along with the manifold (21) are shown in Figure 2-10. The planes separating the four quadrants of the PTO velocity and force are also shown in Figure

2-10. The locus traverses a trajectory that lies on the manifold (21), satisfying the cost objective. The trajectories are also inclined towards the first and fourth octant of the PTO force-velocity space as the controller attempts to actuate the WEC PTO generator to make the PTO force in-phase with the PTO velocity to maximize the PTO power capture.

For the piecewise cost functional of the form (23), the plots for the instantaneous PTO power and the average PTO power are shown in Figure 2-11. For an illustration of piecewise case (23), a PTO cost manifold with only two pieces is considered, as shown in Figure 2-12. The controller is manually switched from one cost manifold to the other at 150 sec. The locus of the PTO force and the PTO velocity, along with the cost manifolds, are shown in Figure 2-12. The locus traverses a trajectory that lies on the manifolds and satisfies the cost objective. In the actual scenarios, the manifold switching would depend upon the current magnitude of PTO force according to (11), as shown in Figure 2-13. The selection of the weight matrix in (15) would depend on the domain interval of the PTO force at any given time. The QP optimization algorithm withstands the manifold switching operation in Figure 12 and converges to an optimal solution. However, with the ACADO toolkit, there is no theoretical guarantee that the optimization routine can always remain safely in its region of convergence [13]. Given that the cost index formulation in (8) includes a convexifying power loss term, for example the power loss surface plots in Figure 2-4, and I_{pto} linear curve fits in Figure 2-3 do not have jump discontinuity at the switching value, the close loop system tends to maintain a stable operation. If the QP problem formulated at a given sample interval is infeasible, the controller will fail to find a solution. This issue can be handled by

monitoring the status of the QP solver during each sampling interval and selecting a suboptimal solution when the QP solver fails.

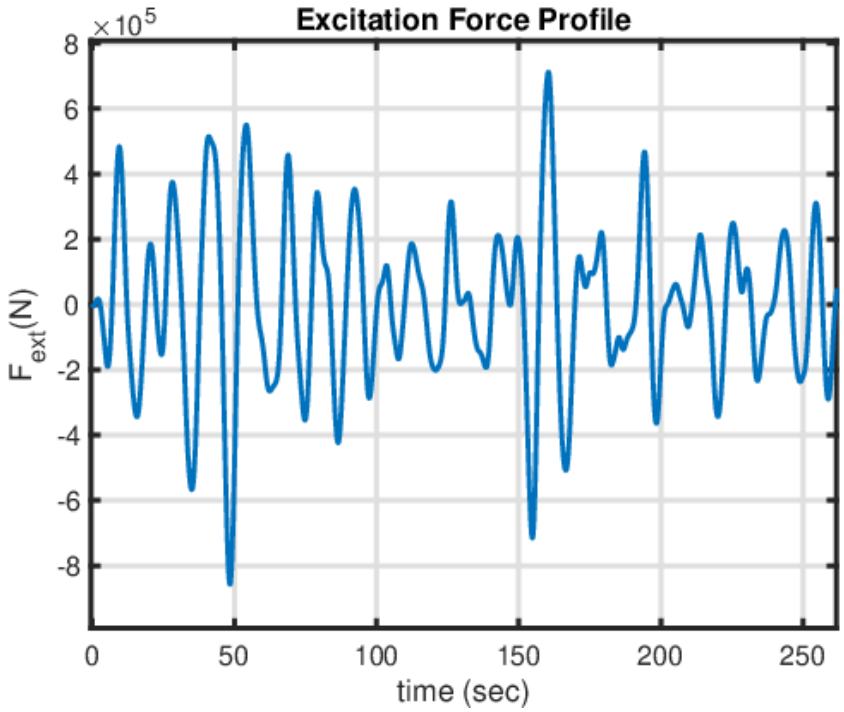

Figure 2-8 Excitation force profile for simulation of the proposed controller.

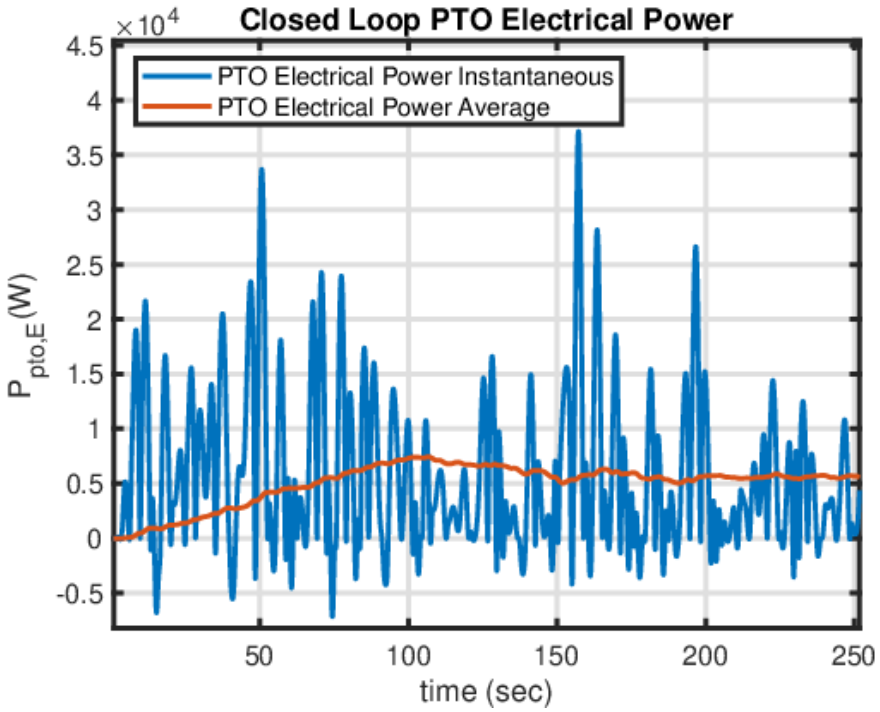

Figure 2-9 Instantaneous and average PTO power output.

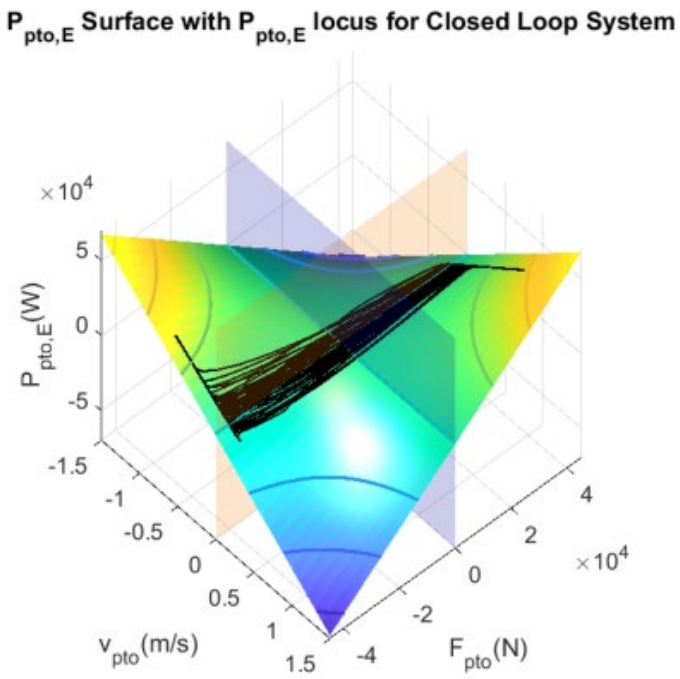

Figure 2-10 The PTO force and PTO velocity locus on the WEC electrical power cost functional.

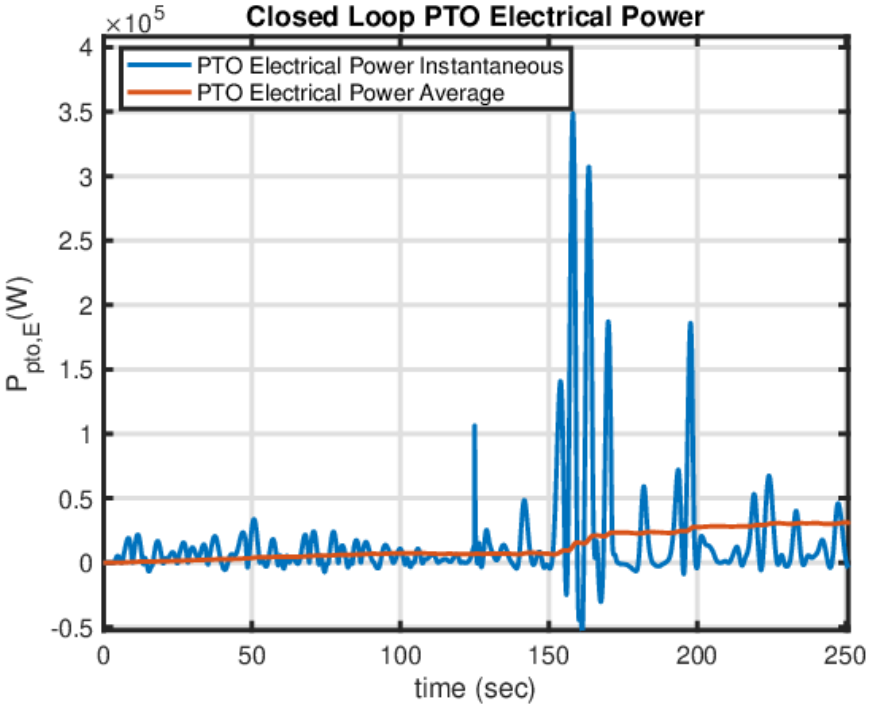

Figure 2-11 Instantaneous and average PTO power output for piecewise nonlinear cost manifold.

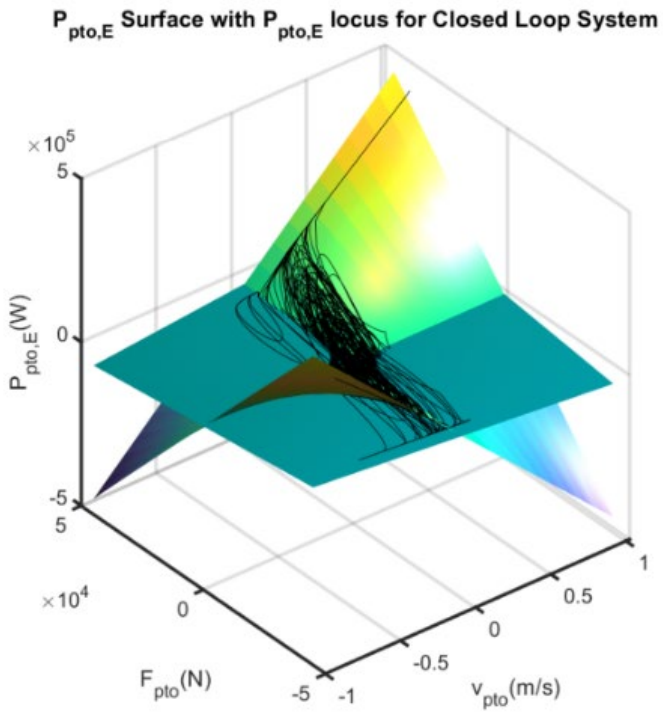

Figure 2-12 The PTO force-velocity locus on piecewise nonlinear cost manifold.

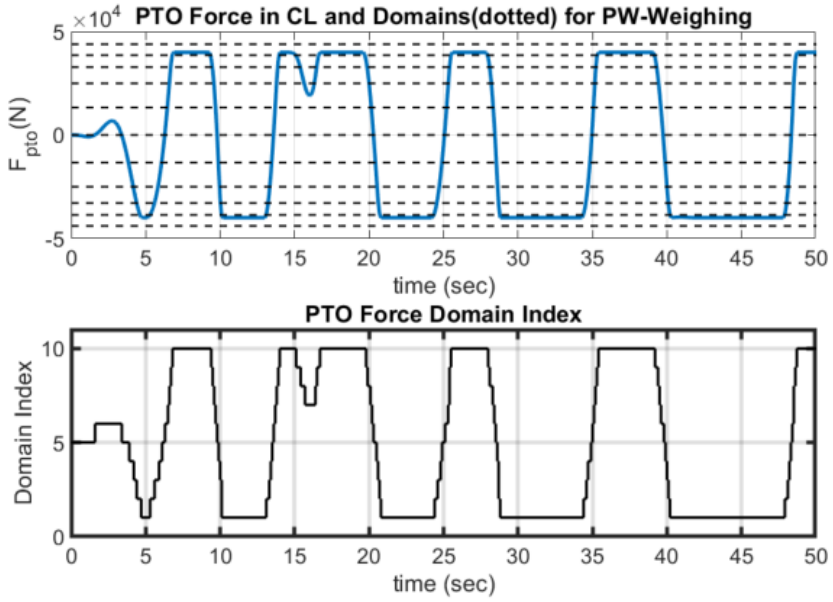

Figure 2-13 The PTO force domains and selection of weight matrix index for cost functional.

The proposed design is implemented on Speedgoat Performance real-time target

machine-109100 [15] with Intel Core i3-3220, 3.3 GHz processor, and 2048 MB of installed RAM. Given the typical ocean wave period of 10 seconds, a sample time of 0.1 seconds was selected for the real-time simulation of NMPC. The Speedgoat based controller implementation is shown in Figure 2-14.

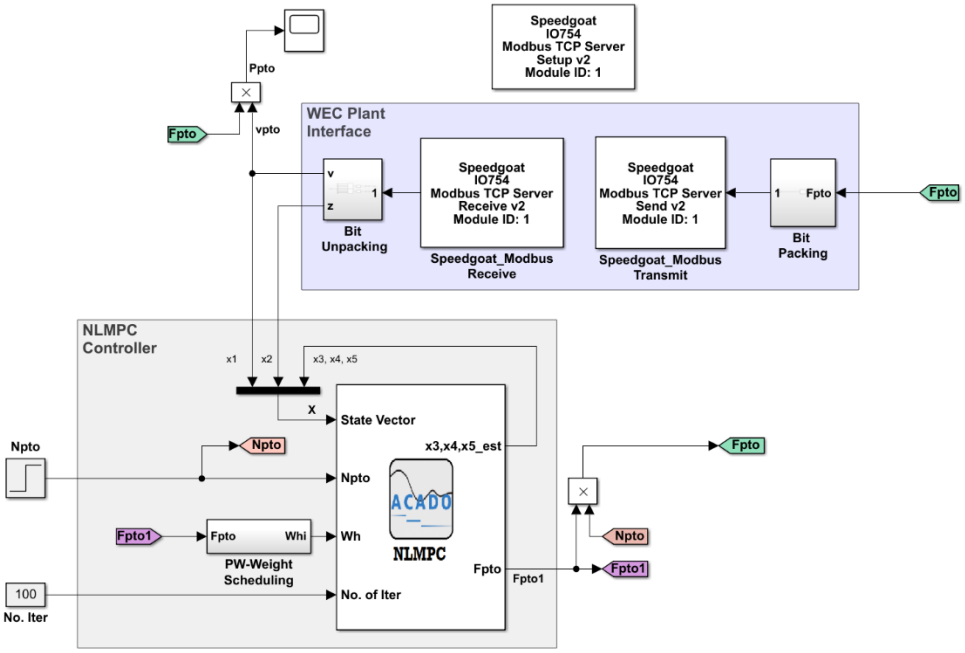

Figure 2-14 Implementation of the proposed NMPC for the Speedgoat real-time target machine.

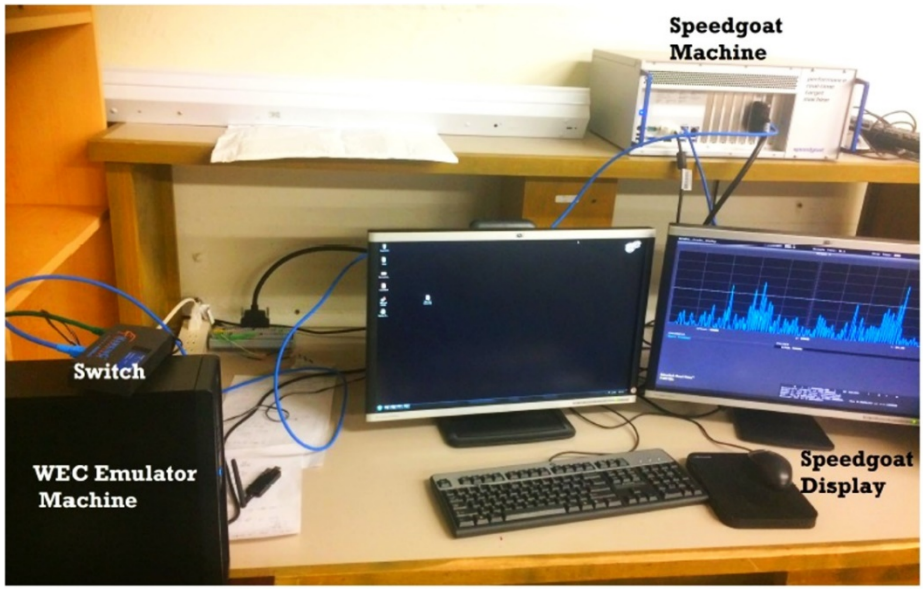

Figure 2-15Testing the controller using real time target machine and the WEC emulator machine.

The target machine is configured to communicate with the WEC plant over the Modbus TCP/IP channel. The WEC dynamics were emulated on another real-time machine, as shown in Figure 2-15. An average of 12% processor load was observed per sampling interval during testing. The real-time implementation of the controller confirmed the simulation results. The updated code has been made publicly available at the following online repository, (github.com/aliSHaider/NMPC_Acado_Simulink_Speedgoat).

2.7 Conclusion

An approach to implement a Nonlinear Model Predictive Controller (NMPC) in real-time with a non-standard cost index is presented. The case study WEC PTO models were presented. The specific PTO power formulations are non-quadratic piecewise functional of the PTO force and PTO velocity. The method of pseudo-quadratization and weight-scheduling is used to implement the NMPC problem using the ACADO toolkit for MATLAB/Simulink. The proposed strategy supports code generation, and the controller was deployed on the Speedgoat Performance real-time target machine-109100, coupled to the real-time WEC emulator machine over the Modbus TCP/IP channel. The proposed methodology successfully maintained an overall feasible operation of the real-time NMPC problem in simulation as indicated by the status port of the NMPC QP-solver. The experimental implementation on the Speedgoat target machine confirmed the optimal power capture results from the simulation with an average of 12% processor load.

2.8 References

1 Muetze, A., Vining, J.G.: 'Ocean Wave Energy Conversion - A Survey', in 'Conference Record of the 2006 IEEE Industry Applications Conference Forty-First

IAS Annual Meeting' Conference Record of the 2006 IEEE Industry Applications Conference Forty-First IAS Annual Meeting, (2006), pp. 1410–1417

2 Brekken, T.K.A.: 'On Model Predictive Control for a point absorber Wave Energy Converter', in '2011 IEEE Trondheim PowerTech' 2011 IEEE Trondheim PowerTech, (2011), pp. 1–8

3 Richter, M., Magaña, M.E., Sawodny, O., Brekken, T.K.A.: 'Power optimisation of a point absorber wave energy converter by means of linear model predictive control'*IET Renewable Power Generation*, 2014, **8**, (2), pp. 203–215.

4 Starrett, M., So, R., Brekken, T.K.A., McCall, A.: 'Increasing power capture from multibody wave energy conversion systems using model predictive control', in '2015 IEEE Conference on Technologies for Sustainability (SusTech)' 2015 IEEE Conference on Technologies for Sustainability (SusTech), (2015), pp. 20–26

5 Richter, M., Magana, M.E., Sawodny, O., Brekken, T.K.A.: 'Nonlinear Model Predictive Control of a Point Absorber Wave Energy Converter'*IEEE Transactions on Sustainable Energy*, 2013, **4**, (1), pp. 118–126.

6 Haider, A.S., Brekken, T.K.A., McCall, A.: 'A State-of-the-Art Strategy to Implement Nonlinear Model Predictive Controller with Non-Quadratic Piecewise Discontinuous Cost Index for Ocean Wave Energy Systems', in '2020 IEEE Energy Conversion Congress and Exposition (ECCE)' 2020 IEEE Energy Conversion Congress and Exposition (ECCE), (2020), pp. 1873–1878

7 Li, G.: 'Nonlinear model predictive control of a wave energy converter based on differential flatness parameterisation'*International Journal of Control*, 2017, **90**, (1), pp. 68–77.

8 Bacelli, G., Genest, R., Ringwood, J.V.: 'Nonlinear control of flap-type wave energy converter with a non-ideal power take-off system'*Annual Reviews in Control*, 2015, **40**, pp. 116–126.

9 Jia, Y., Meng, K., Dong, L., Liu, T., Sun, C., Dong, Z.Y.: 'Economic Model Predictive Control of a Point Absorber Wave Energy Converter'*IEEE Transactions on Sustainable Energy*, 2021, **12**, (1), pp. 578–586.

10 Angeli, D., Amrit, R., Rawlings, J.B.: 'On Average Performance and Stability of Economic Model Predictive Control'*IEEE Transactions on Automatic Control*, 2012, **57**, (7), pp. 1615–1626.

11 Quirynen, R., Vukov, M., Zanon, M., Diehl, M.: 'Autogenerating microsecond solvers for nonlinear MPC: A tutorial using ACADO integrators'*Optimal Control Applications and Methods*, 2015, **36**, (5), pp. 685–704.

12 Houska, B., Ferreau, H.J., Diehl, M.: 'ACADO toolkit—An open-source framework for automatic control and dynamic optimization'*Optimal Control Applications and Methods*, 2011, **32**, (3), pp. 298–312.

13 Starrett, M., So, R., Brekken, T.K.A., McCall, A.: 'Development of a state space model for wave energy conversion systems', in '2015 IEEE Power Energy Society General Meeting' 2015 IEEE Power Energy Society General Meeting, (2015), pp. 1–5

14 'Marine and Hydrokinetic Data Repository (MHKDR)', https://mhkdr.openei.org/, accessed May 2021

15 'Speedgoat - The Quickest Path to Real-Time Simulation and Testing', https://www.speedgoat.com/, accessed February 2021

3 Manuscript 2:

Real-time Nonlinear Model Predictive Controller for Multiple Degrees of Freedom Wave Energy Converters with Non-ideal Power Take-off

Ali S. Haider, Ted K.A. Brekken, Alan McCall

Journal of Marine Science and Engineering

St. Alban-Anlage 66, 4052 Basel, Switzerland

18 August 2021

3.1 Abstract

An increase in Wave Energy Converter (WEC) efficiency requires not only consideration of the nonlinear effects in the WEC dynamics and the Power Take-off (PTO) mechanisms but also to treat the whole system in an integrated way, i.e., the buoy dynamics, the PTO system, the control strategy. It results in an optimization formulation that has a nonquadratic and nonstandard cost functional. This article presents the application of real-time Nonlinear Model Predictive Controller (NMPC) to two degrees of freedom point absorber type WEC with highly nonlinear PTO characteristics. The nonlinear effects such as the fluid viscous drag are also included in the plant dynamics. The controller is implemented on a real-time target machine, and the WEC device is emulated in real-time using the WECSIM toolbox. The results for the successful performance of the design are presented for irregular waves under linear and nonlinear hydrodynamic conditions.

3.2 Introduction

Renewable energy technologies present a viable, sustainable contribution to the world's growing energy demands, and the ocean provides a potential for an enormous untapped energy resource for the world's energy portfolio [1,2]. The prospect of ocean wave energy has triggered research in optimal power capture techniques for wave energy converters, including non-ideal operating conditions, such as the non-ideal PTO system constraints [3] and nonlinear sea conditions. Achieving optimal power capture by a WEC in practice is a multifaceted objective. It depends on various factors such as the physical design of the WEC, the design of the PTO system, the ocean conditions, and the control techniques.

Model Predictive Control (MPC) is a promising control approach for wave energy converters' relatively slow plant dynamics because it maximizes energy capture while respecting the system's mechanical limits. MPC is a look ahead control strategy that predicts future system behavior to solve a constrained optimization problem and determines the best control action to maximize the output power of WEC. MPC and other optimal control schemes such as pseudospectral methods and MPC-like algorithms have been comprehensively studied in the literature for a single WEC device and an array of wave energy converters [4–10]. An MPC algorithm uses an internal model of the plant to predict the system's future states [11]. Nonlinear control algorithms can consider the non-ideal operating conditions and nonlinear effects, including but not limited to non-ideal power take-off mechanism [12], nonlinear viscous drag terms [13,14], and nonlinear mooring dynamics [2]. The non-ideality of PTO systems in most literature is limited to the efficiency of the PTO mechanism [14–17]. One of the motivations for this research is to consider higher-order nonlinear PTO characteristics as an optimization objective for the NMPC problem. The Economic MPC techniques consider a general economic cost function directly in real-time [18–20]. However, we have deployed a Real-time Iterative (RTI) algorithm [21,22] to optimize a more general class of non-ideal PTO mechanism using pseudo-quadratic formulations [3], and this method also supports nonlinearities in the plant dynamics, such as mooring and fluid viscous drag. Another motivation for this work is investigating nonlinear multiple degrees of freedom WEC coupled to non-ideal PTO.

Lots of work has been focused on studying multiple degrees of freedom WEC devices that prove a significant improvement of power capture by the WEC device.

Multi-resonant feedback control of a three degree of freedom WEC is presented [23], where a linear hydrodynamic model is considered, and multi-resonant proportional-derivative control law is proposed where the focus is linear plant dynamics under unconstrained control. An analysis of a multi-degree-of-freedom point absorber WEC in the surge, heave, and pitch directions is presented in [24], and frequency and time-domain formulations are presented for the linear plant dynamics. A time-domain model for a point absorber WEC in six degrees of freedom is developed in [25] with an optimal resistive loading. The three degrees of freedom model of a WEC is presented in [26], where the capture performance of various PTO systems is investigated for a linear plant model. An Active control strategy based on the optimal velocity trajectory tracking for a multi-DoF submerged point absorber WEC is presented in [27], where a linearized dynamic system model is considered along with an ideal PTO mechanism. A nonlinear MPC design and implementation based on differential flatness parameterization has been proposed in [28]. Given that most of the work focused on linear plant dynamics for multiple degrees of freedom WEC or ideal PTO mechanisms, and lack of application of NMPC for such class or problems, we have investigated the application of NMPC to nonlinear multiple DoF WEC plant with a non-ideal PTO mechanism, and focus being the real-time implementation of the control algorithm on a real-time target machine.

This research presents the maximization of power extraction by a 2-DoF WEC device, a WECSIM [29] model of the full-scale version of the Dehlsen Associates, LLC multi-pod CENTIPOD [30]. Although the CENTIPOD device is an array device, the cross-coupling between pods is ignored for this study, which is negligible for the sea

conditions of interest in this work and will be investigated in the future. The goal is to optimize the power extracted by the heave and pitch PTOs subject to actuation and velocity constraints. The objective function is a nonstandard and nonquadratic functional of PTO force and velocity, resulting from a practical PTO generator power loss characteristic. The WEC model includes nonlinear viscous drag terms; hence the resulting plant model is a nonlinear dynamic system. We have implemented an NMPC for the problem. To tackle a free-formed objective function subjected to nonlinear system dynamics, we have used the extended version of the NMPC design from [31], based on Pseudo-Quadratization using Acado Toolkit [22]. No prior knowledge of wave excitation is assumed. The WEC model is simulated on a real-time emulator machine, while control is deployed on Speedgoat real-time performance machine [32], which is interfaced with the WEC emulator machine through an ethernet port. The simulation results for real-time NMPC are presented for the linear and nonlinear hydrodynamics conditions simulated in WECSIM.

3.3 Time Domain Model of a Multiple Degree of Freedom WEC

The WEC device is a full-scale version of the Dehlsen Associates, LLC multi-pod CENTIPOD [30,33]. A 1:35-scale version of the device is shown in Figure 3-1. This CENTIPOD device has three floating pods and three spars fixed to a backbone structure. The backbone is anchored using mooring lines, as shown in Figure 2. In its 2-DoF version, each pod is attached to a PTO mechanism in the heave and pitch degrees of freedom. All pods in Figure 3-2 are assumed identical. Since the CENTIPOD device is an array device, the array effect [34] could become prominent as the significant

height of the waves increases and the incident angle of the waves is not parallel to the x-axis in Figure 3-2.

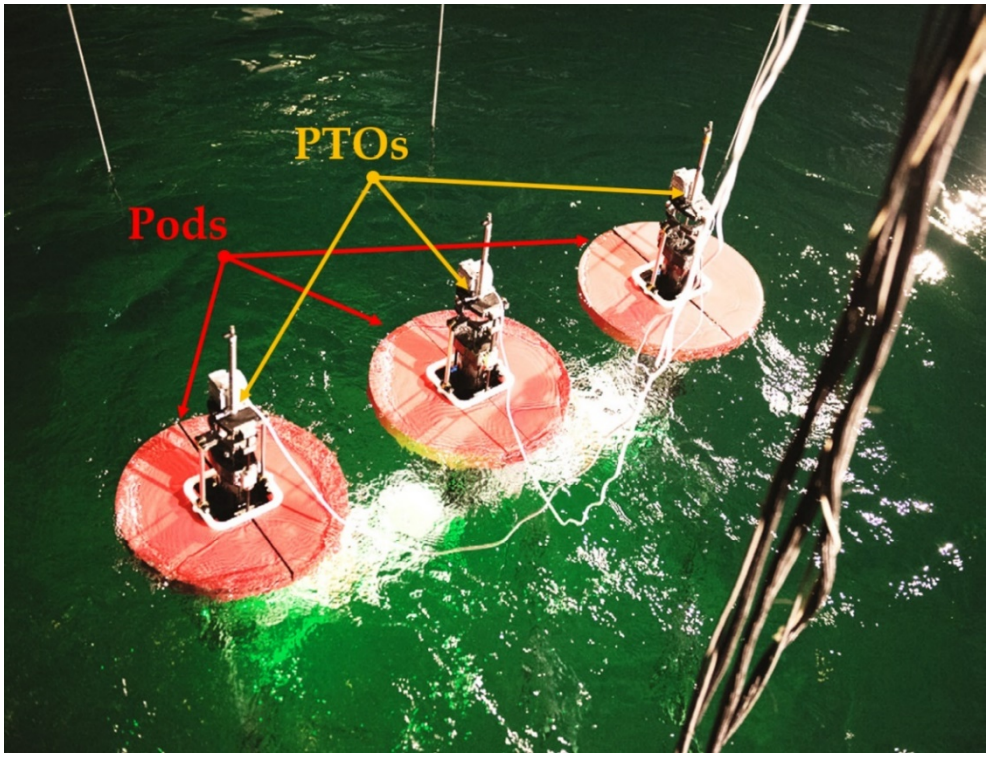

Figure 3-1 Image of the Dehlsen Associates, LLC, 1:35-scale CENTIPOD WEC.

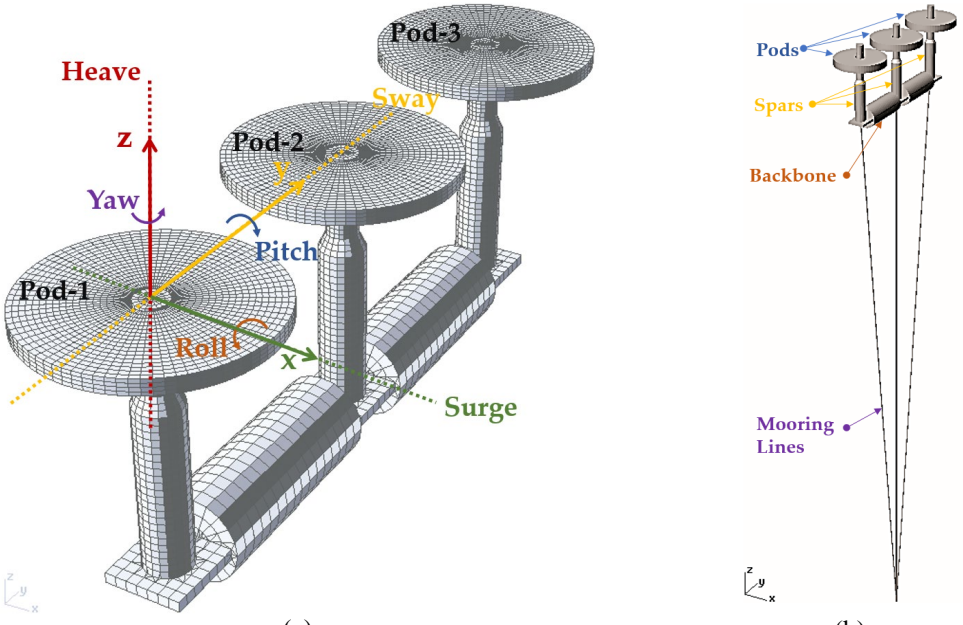

Figure 3-2 Degrees of freedom for dynamic modelling of CENTIPOD WEC: (a) baseline configuration; (b) model with mooring lines.

For this study, incident waves are assumed parallel to the x-axis, and for the sea state of interest in this work, the cross-coupling between the pods is very small and is neglected, although it will be investigated in future work.

We will follow the subscript notation of WEC-Sim Toolbox [29] for the degrees of freedom for WEC, in which the integers from 1,2,.. 6 correspond to surge, sway, heave, roll, pitch, and yaw, respectively. Some other notations and symbols for WEC Modeling are given in Table 3-1.

3.4 Surge-Pitch-Heave Model of WEC Modeling in State-Space Form

Each pod in Figure 3-2 is modeling as a wave point absorber device. The Cummins equation for the coupled surge and pitch dynamics for a point absorber pod (assuming a local reference frame) is given by,

$$\begin{aligned}\big(m + A_{11}(\infty)\big)\dot{v}_1 + A_{15}(\infty)\dot{v}_5 \\ = -F_{r,11}(t) - F_{r,15}(t) - F_{v,1}(t) + F_{e,1}(t)\end{aligned} \tag{1a}$$

$$\begin{aligned}\big(m + A_{55}(\infty)\big)\dot{v}_5 + A_{51}(\infty)\dot{v}_1 \\ = -F_{r,55}(t) - F_{r,51}(t) - F_{v,5}(t) - F_{hs,5}(t) - F_{p,5}(t) \\ + F_{e,5}(t)\end{aligned} \tag{1b}$$

The Cummins equation for the heave dynamics of a point absorber pod is given by,

$$\begin{aligned}\big(m + A_{33}(\infty)\big)\dot{v}_3(t) \\ = -F_{r,33}(t) - F_{hs,3}(t) - F_{v,3}(t) - F_{p,3}(t) + F_{e,3}(t)\end{aligned} \tag{2}$$

Table 3-1 Notations and symbols for WEC modelling.

Variable	Description
v_i	Velocity (Linear or Angular) in i^{th} DoF
x_i	Displacement (Linear or Angular) in i^{th} DoF
ξ_i	Intermediate State variables for radiation force State-Space approximation
$F_{r,pq}$	Radiation force in p^{th} DoF due to velocity in q^{th} DoF
$F_{hs,i}$	Hydrostatic force in i^{th} DoF
$F_{v,i}$	Viscous drag force in i^{th}DoF
$F_{e,i}$	Wave excitation force in i^{th}DoF
$F_{p,i}$	PTO force in i^{th}DoF
m	Mass of the float
$A_{pq}(\infty)$	Added mass at the infinite frequency in p^{th} DoF due to acceleration in q^{th} DoF
C_i	The hydrostatic restoring coefficient in i^{th} DoF
$C_{vd,i}$	Viscous drag coefficient in i^{th} DoF
A_{qp}	Frequency-dependent added mass in p^{th} DoF due to acceleration in q^{th} DoF
B_{qp}	Frequency-dependent damping in p^{th} DoF due to velocity in q^{th} DoF
K_{pq}	Radiation force impulse response without infinite frequency added mass
Z_{qp}	WEC Intrinsic impedance response in p^{th} DoF due to velocity in q^{th} DoF
a_i	Polynomial coefficients
$c_{i,j}$	Polynomial coefficients for cost functional
$I_{p,i}$	i^{th} PTO current
η_{Conv}	PTO converter efficiency
K_{Cu}	PTO generator copper loss constant
R_Ω	PTO generator winding resistance

The hydrostatic, viscous damping, and radiation force terms in (1) and (2) are given by,

$$F_{r,ij}(t) = \int_{-\infty}^{t} K_{ij}(t-\tau) v_j d\tau \tag{3a}$$

$$F_{hs,i}(t) = C_i x_i \tag{3b}$$

$$F_{v,i}(t) = C_{d,i} v_i |v_i| \tag{3c}$$

A transfer function expression can approximate the convolution integral term in (3),

$$F_{r,pq}(t) = \int_{-\infty}^{t} K_{pq}(t-\tau) v_q d\tau \Leftrightarrow F_{r,pq}(j\omega) = Z_{pq}(j\omega) V_q(j\omega) \tag{4}$$

Using the device data from WAMIT [35], we can approximate the intrinsic impedance $Z_{pq}(j\omega)$ in (4) by a second order transfer function using System Identification techniques,

$$\begin{aligned} Z_{pq}(j\omega) &= \left[j\omega \left(A_{pq}(j\omega) - A_{pq}(\infty) \right) + B_{qp}(j\omega) \right] \\ &\approx \left. \frac{\alpha_{pq,1} s + \alpha_{pq,0}}{s^2 + \beta_{pq,1} s + \beta_{pq,0}} \right|_{s=j\omega} \end{aligned} \tag{5}$$

Using (5) in (4) enables us to express the radiation force as a second-order transfer function,

$$F_{r,pq}(s) \approx \frac{\alpha_{pq,1} s + \alpha_{pq,0}}{s^2 + \beta_{pq,1} s + \beta_{pq,0}} V_q(s) \tag{6}$$

The transfer function expression in (6) can be converted to the State-Space expressions in the Observer-Canonical forms for each of the radiation force terms,

$$\begin{bmatrix} \dot{\xi}_k(t) \\ \dot{\xi}_{k+1}(t) \end{bmatrix} = \begin{bmatrix} 0 & 1 \\ a_k & a_{k+1} \end{bmatrix} \begin{bmatrix} \xi_k(t) \\ \xi_{k+1}(t) \end{bmatrix} + \begin{bmatrix} b_k \\ b_{k+1} \end{bmatrix} v_q(t) \tag{7a}$$

$$y_{pq}(t) = [1 \quad 0] \begin{bmatrix} \xi_k(t) \\ \xi_{k+1}(t) \end{bmatrix} \approx F_{r,pq}(t) \tag{7b}$$

By the comparison of (6) and (7), we have, $\alpha_{pq,1} = b_k$, $\beta_{pq,1} = -a_{k+1}, \beta_{pq,0} = -a_k$, and $\alpha_{pq,0} = b_{k+1} - b_k a_{k+1}$. Making a change of variables in (1),

$$M_{ii} = \left(m + A_{ii}(\infty)\right) \tag{8a}$$

$$F_{1,net} = -F_{r,11}(t) - F_{r,15}(t) - F_{v,1}(t) + F_{e,1}(t) \tag{8b}$$

$$F_{5,net} = -F_{r,55}(t) - F_{r,51}(t) - C_5 x_5 - F_{v,5}(t) - F_{p,5}(t) + F_{e,5}(t) \tag{8c}$$

Using (8) in (1), we get the pitch-surge coupled model of a pod as,

$$\begin{bmatrix} \dot{v}_1 \\ \dot{v}_5 \end{bmatrix} = \begin{bmatrix} M_{11} & A_{15}(\infty) \\ A_{51}(\infty) & M_{55} \end{bmatrix}^{-1} \begin{bmatrix} F_{1,net} \\ F_{5,net} \end{bmatrix} \tag{9a}$$

The viscous drag force term $v_i|v_i|$ in (3c) is a hard nonlinearity that may lead to convergence issues for the optimization solvers. One solution is to approximate this term with a soft nonlinearity by replacing it with a smooth higher-order polynomial. A third-order polynomial approximation for $v_i|v_i|$ is used in the surge and heave direction, where the range of interest of velocity is $v_i \in (-1.5,1.5)\ m/sec$, and a fifth-order polynomial approximation is used for pitch direction, where the range of interest of velocity is $v_i \in (-0.5,0.5)\ rad/sec$. With, $p_{i,j}$ being the j^{th} polynomial coefficient for i^{th} degree polynomial curve fit,

$$F_{v,i} = C_{d,i} v_i |v_i| \approx C_{d,i}\left(p_{3,3} v_i^3 + p_{3,1} v_i\right), \qquad i = 1,3, \tag{10a}$$

$$F_{v,5} = C_{d,5} v_5 |v_5| \approx C_{d,5}\left(p_{5,5} v_5^5 + p_{5,3} v_5^3 + p_{5,1} v_5\right) \tag{10b}$$

The curve fits (10a) and (10b) are shown in Figure 3(a) and Figure 3(b), respectively. Using (9) and (2), we get a Surge-Heave-Pitch model of a pod as,

$$\dot{\mathbf{X}} = \mathbf{A}\mathbf{X} + \mathbf{B_p}\mathbf{F_p} + \mathbf{B_v}\mathbf{F_v} + \mathbf{B_e}\mathbf{F_e} \tag{11}$$

where,

$$\mathbf{F_p} = [F_{p,5} \quad F_{p,3}]^T \tag{12a}$$

$$\mathbf{F_v} = [F_{v,1} \quad F_{v,5} \quad F_{v,3}]^T \tag{12b}$$

$$\mathbf{F_e} = [F_{e,1} \quad F_{e,5} \quad F_{e,3}]^T \tag{12c}$$

$$\mathbf{X} = [v_1 \quad v_5 \quad x_5 \quad \xi_3 \quad \xi_4 \quad \xi_5 \quad \xi_6 \quad \xi_7 \quad \xi_8 \quad \xi_9 \quad \xi_{10} \quad v_3 \quad x_3 \quad \xi_1 \quad \xi_2]^T \tag{12d}$$

and the radiation force terms are approximated by following state variables using (7),

$$F_{r,11} = \xi_3,\ F_{r,15} = \xi_5,\ F_{r,51} = \xi_7,\ F_{r,55} = \xi_9,\ F_{r,33} = \xi_1. \tag{13}$$

and,

$$\mathbf{A} = \begin{bmatrix} \mathbf{A_{15}} & \mathbf{0} \\ \mathbf{0} & \mathbf{A_{33}} \end{bmatrix}$$

$$\mathbf{A_{33}} = \begin{bmatrix} 0 & \frac{-C_3}{M_{33}} & \frac{-1}{M_{33}} & 0 \\ 1 & 0 & 0 & 0 \\ b_1 & 0 & 0 & 1 \\ b_2 & 0 & a_1 & a_2 \end{bmatrix} \tag{14a}$$

$$\mathbf{A_{15}} = \begin{bmatrix} 0 & 0 & -m_{15}C_5 & -m_{11} & 0 & -m_{11} & 0 & -m_{15} & 0 & -m_{15} & 0 \\ 0 & 0 & -m_{55}C_5 & -m_{51} & 0 & -m_{51} & 0 & -m_{55} & 0 & -m_{55} & 0 \\ 0 & 1 & 0 & 0 & 0 & 0 & 0 & 0 & 0 & 0 & 0 \\ b_3 & 0 & 0 & 0 & 1 & 0 & 0 & 0 & 0 & 0 & 0 \\ b_4 & 0 & 0 & a_3 & a_4 & 0 & 0 & 0 & 0 & 0 & 0 \\ 0 & b_5 & 0 & 0 & 0 & 0 & 1 & 0 & 0 & 0 & 0 \\ 0 & b_6 & 0 & 0 & 0 & a_5 & a_6 & 0 & 0 & 0 & 0 \\ 0 & b_7 & 0 & 0 & 0 & 0 & 0 & 0 & 1 & 0 & 0 \\ 0 & b_8 & 0 & 0 & 0 & 0 & 0 & a_7 & a_8 & 0 & 0 \\ b_9 & 0 & 0 & 0 & 0 & 0 & 0 & 0 & 0 & 0 & 1 \\ b_{10} & 0 & 0 & 0 & 0 & 0 & 0 & 0 & 0 & a_9 & a_{10} \end{bmatrix} \quad (14b)$$

$$\mathbf{B_p} = \begin{bmatrix} -m_{15} & 0 \\ -m_{55} & 0 \\ 0 & 0 \\ 0 & 0 \\ 0 & 0 \\ 0 & 0 \\ 0 & 0 \\ 0 & 0 \\ 0 & 0 \\ 0 & 0 \\ 0 & \frac{-1}{M_{33}} \\ 0 & 0 \\ 0 & 0 \\ 0 & 0 \end{bmatrix}, \mathbf{B_v} = \begin{bmatrix} -m_{11} & -m_{15} & 0 \\ -m_{51} & -m_{55} & 0 \\ 0 & 0 & 0 \\ 0 & 0 & 0 \\ 0 & 0 & 0 \\ 0 & 0 & 0 \\ 0 & 0 & 0 \\ 0 & 0 & 0 \\ 0 & 0 & 0 \\ 0 & 0 & 0 \\ 0 & 0 & \frac{-1}{M_{33}} \\ 0 & 0 & 0 \\ 0 & 0 & 0 \\ 0 & 0 & 0 \end{bmatrix}, \mathbf{B_e} = \begin{bmatrix} m_{11} & m_{15} & 0 \\ m_{51} & m_{55} & 0 \\ 0 & 0 & 0 \\ 0 & 0 & 0 \\ 0 & 0 & 0 \\ 0 & 0 & 0 \\ 0 & 0 & 0 \\ 0 & 0 & 0 \\ 0 & 0 & 0 \\ 0 & 0 & 0 \\ 0 & 0 & \frac{1}{M_{33}} \\ 0 & 0 & 0 \\ 0 & 0 & 0 \\ 0 & 0 & 0 \end{bmatrix} \quad (14b)$$

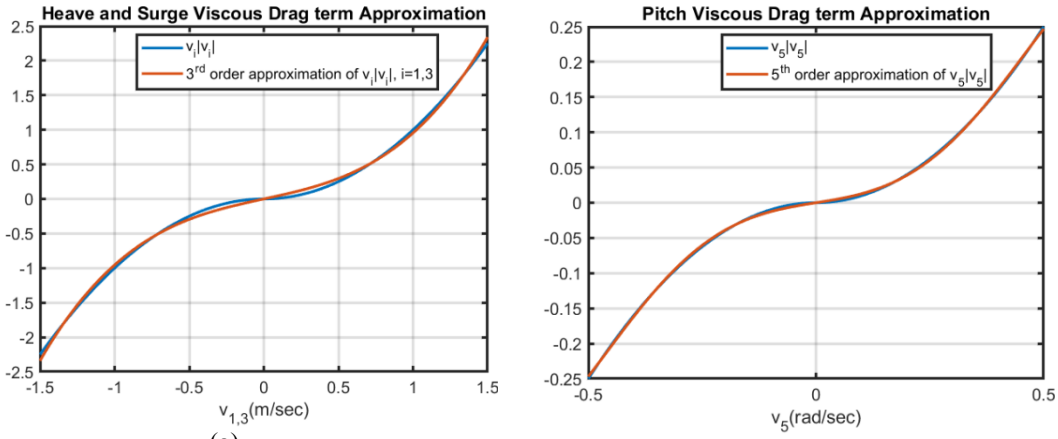

(a) (b)

Figure 3-3 Polynomial approximations of the quadratic drag term $\boldsymbol{v_i|v_i|}$: (a) 3rd order curve fit for heave and surge axes; (b) 5th order curve fit for pitch axis.

Substituting (10) in (11) gives us a 2-DoF (Heave and Pitch) WEC nonlinear plant model, where the surge is coupled with the pitch and heave is a decoupled DoF. We can use this plant model as a prediction model in NMPC.

3.5 Nonquadratic WEC-PTO Model

The electrical power output from the PTO mechanism of the WEC is the difference between the mechanical power input from the waves and the losses in the PTO system. For a given PTO generator, the electrical PTO power cost functional to be maximized, including the electrical losses, is given by,

$$\begin{aligned} \max_{F_{p,i}} P_{E,i} &= \eta_{Conv}\left(P_{Mechanical,i} - P_{Loss,i}\right) \\ &= \eta_{Conv}\left(F_{p,i}v_i - K_{Cu}\left[I_{p,i}\left(F_{p,i}\right)\right]^2 R_{\Omega}\right), \end{aligned} \tag{15}$$

The case study scenario is taken from McCleer Power's Linear PTO generator [3] with the PTO force-current characteristics given by Figure 3-4. We can approximate the experimental data in Figure 4 with a mathematical relation, such as a piecewise linear function or a nonlinear function. We have used polynomial approximation which is a smooth function. This relation is described by a third-order curve fit between the PTO current and the PTO force,

$$I_{p,i}\left(F_{p,i}\right) = a_{3,i}F_{p,i}^3 + a_{2,i}F_{p,i}^2 + a_{1,i}F_{p,i} + a_{0,i}, \tag{16}$$

Putting (16) in (15), we get,

$$P_{E,i} = c_{0,i}F_{p,i}v_i - (c_{1,i}F_{p,i}^6 + c_{2,i}F_{p,i}^5 + c_{3,i}F_{p,i}^4 + c_{4,i}F_{p,i}^3 + c_{5,i}F_{p,i}^2 + c_{6,i}F_{p,i} + c_{7,i}), \tag{17}$$

The PTO cost functional surface in (17) is plotted in the PTO velocity-force plane, as shown in Figure 5. The surface plot of the mechanical PTO power, $P_{Mechanical,i} =$

$F_{p,i}v_i$ is non-convex, as shown in Figure 5. However, the electrical PTO power surface, $P_{E,i}$ in (15) has a quadratic power loss term, and it gives convexity to the electrical power surface along the PTO force axis in Figure 5.

3.6 Implementation of NMPC for 2-DoF Heave-Pitch WEC

The optimal control problem of a WEC involves manipulating the PTO force/torque to maximize the power capture while respecting some system constraints. Various optimal control approaches have been developed, and a comprehensive review can be found in [36]. MPC is a model-based online optimal control solution, and a given NMPC problem optimizes a manipulated variable $\mathrm{u}(t)$ to maximize some cost functional $\mathrm{P}(\cdot)$ while respecting the system constraints. A special class of NMPC problems has been formulated in [31,37], in which the cost functional takes on a nonlinear piecewise polynomial form. Considering the case of finite-horizon optimization control, we can mathematically describe the NMPC problem of such a class as,

$$\underset{\mathbf{u}(t)}{maximize}\ \mathbf{P}\big[t, \dot{\mathbf{X}}(t), \mathbf{X}(t), \mathbf{U}(t), \mathbf{p}(t)\big] \tag{18}$$

$$\text{Where: } \mathbf{P}(\cdot) = \begin{cases} P_1(\cdot) + \rho_{N,1}(\cdot), & q_k(t) < R_1 \\ P_2(\cdot) + \rho_{N,2}(\cdot), & R_1 \le q_k(t) \le R_2 \\ \vdots & \vdots \\ P_j(\cdot) + \rho_{N,j}(\cdot), & R_{j-1} \le q_k(t) \le R_j \end{cases}, \tag{19}$$

subject to,

$$\text{Dynamic Constraints: } \mathbf{0} = \mathbf{g}\big(t, \dot{\mathbf{X}}(t), \mathbf{X}(t), \mathbf{U}(t), \mathbf{d}(t), \mathbf{p}(t), N\big), \tag{20a}$$

Boundary Constraint Function:

$$\mathbf{0} = \mathbf{r}(N, \mathbf{X}(0), \mathbf{U}(0), \mathbf{X}(N), \mathbf{U}(N), \mathbf{p}), \tag{20b}$$

Path Constraints Function: $0 \geq \mathbf{s}(t, \mathbf{X}(t), \mathbf{U}(t), \mathbf{p}(t))$. (20d)

The description of various variables and constants in (18) through (20) is given in Table. 3-2. The wave excitation force $\mathbf{F_e}$ acting on the hull is considered an unmeasured system disturbance, and based on the available measurements, the controller internally estimates $\mathbf{F_e}$.

For the 2-DoF (heave-pitch) WEC problem, the objective function to be maximized in (17) will be the sum of electrical PTO power output in the heave and pitch DoFs for each pod,

$$P_E = P_{E,3} + P_{E,5}, \tag{21}$$

Table 3-2 Symbols and notations for NMPC formulation.

Variable	Description
N	Prediction horizon
X	State vector
$\rho_{N,i}$	Finite horizon terminal cost penalty or Mayer terms
$P_i(\cdot)$	Some Nonlinear functions or Lagrange terms
p	A column vector of time-varying parameters
U	PTO Force manipulated variable vector, $\mathrm{F_p}(N)$
d	Excitation force disturbance vector, $\mathrm{F_e}$ (N)
$q_k(t)$	Cost functional scheduling variable
R_i	Some real numbers, such that $R_{k+1} > R_k$

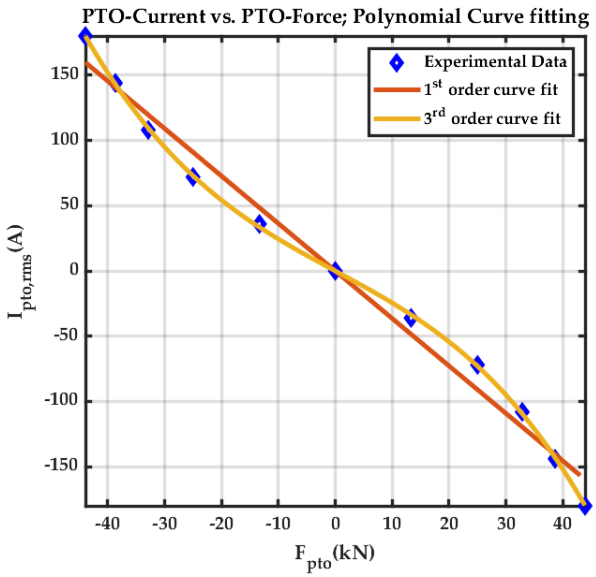

Figure 3-4 Polynomial curve fitting to the PTO force-current experimental data for a PTO generator.

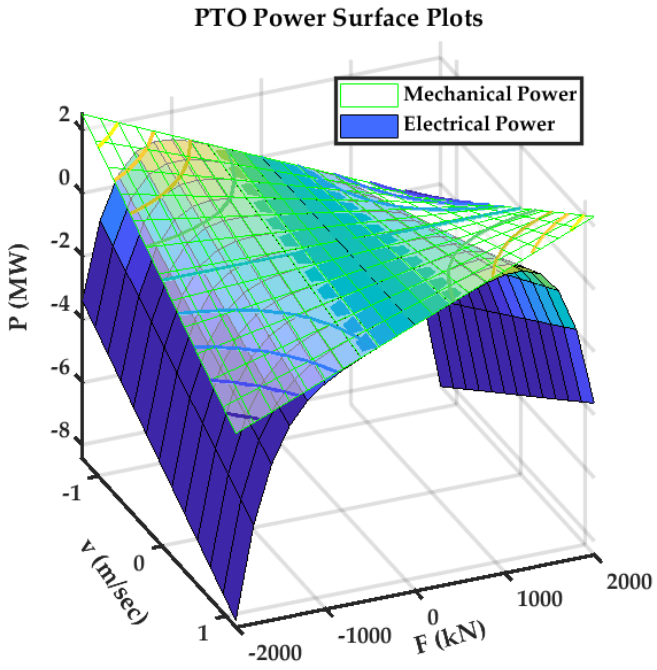

Figure 3-5 Mechanical and electrical PTO power surface plot in PTO velocity-force plane.

Using the technique developed in [31], we can put (21) into Pseudo-Quadratic form by defining a suitable $\mathbf{h_i}$ vector for heave and pitch as,

$$\mathbf{h_i} = \begin{bmatrix} F_{p,i}^3 & F_{p,i}^2 & F_{p,i} & v_i & 1 \end{bmatrix}^T, \qquad i = 3,5 \tag{22}$$

with,

$$\mathbf{h} = \begin{bmatrix} \mathbf{h_3} \\ \mathbf{h_5} \end{bmatrix}, \tag{23}$$

we can reformulate (21) as,

$$P_E = \frac{1}{2}\mathbf{h^T}\left(2\begin{bmatrix} \mathbf{W_3} & \mathbf{0} \\ \mathbf{0} & \mathbf{W_5} \end{bmatrix}\right)\mathbf{h} = \frac{1}{2}\mathbf{h^T}(2\mathbf{W})\mathbf{h}, \tag{24}$$

By using (17) in (21), the weighting matrix **W** can be obtained by polynomial decomposition of (21) by the vector **h** in (23) as the basis vector,

$$\mathbf{W_i} = \frac{1}{2}\begin{bmatrix} -2c_{1,i} & -c_{2,i} & 0 & 0 & 0 \\ -c_{2,i} & -2c_{3,i} & -c_{4,i} & 0 & 0 \\ 0 & -c_{4,i} & -2c_{5,i} & c_{0,i} & -c_{6,i} \\ 0 & 0 & c_{0,i} & 0 & 0 \\ 0 & 0 & -c_{6,i} & 0 & -2c_{7,i} \end{bmatrix}, \qquad i = 3,5 \tag{25}$$

The controller is implemented using Acado toolkit [22] following the approach developed in [3].

3.7 Results

The schematic diagram of the test setup is shown in Figure 3-6. The corresponding hardware setup is shown in Figure 3-7. NMPC is designed in the host machine, which generated code and deployed the controller to the Speedgoat Performance real-time target machine [32], model-109100 with Intel Core i3 3.3 GHz, two cores, and 2048MB DDR3 RAM. The Speedgoat machine is interfaced with a real-time WEC emulator machine through an Ethernet Universal Data Port (UDP) channel. The three WEC pods in Figure 3-1 are assumed identical, and the same controller is implemented for each

pod as shown in Figure 3-8, while the cross-coupling between pods is ignored for this work. The physical velocity and force constraints of the PTO mechanisms imposed as $|v_3| \leq 2\ m/sec$, $|v_5| \leq 0.5\ rad/sec$ and $\left|F_{p,i}\right| \leq 400kN$. The emulated WEC-Sim model of CENTIPOD device is shown in Figure 3-9.

Since the WEC pods are assumed identical with no cross-coupling, results are presented only for a single pod. The sea state of interest for WEC-Sim is given in Table 3-3. This particular sea state's selection is based on the future testing site of interest for the WEC device, although the hardware testing and a more elaborated study involving other sea states are planned for the future. A step time of $0.1\ sec$ is used for MPC formulation, close to one-tenth of the peak wave period. The performance of NMPC is compared against the linear MPC, and the analysis is performed for the linear and nonlinear hydrodynamics sea conditions.

The average electrical power output results for the heave and pitch PTOs for 2-DoF pod-1 are shown in Figure 3-10(a) and Figure 3-10(b), respectively, for linear MPC and NMPC subjected to Linear hydrodynamic conditions. Here we have considered Exponentially Weighted Moving Average (EWMA) with the forgetting factor set to unity. The instantaneous electrical power output results corresponding to Figure 3-10 are shown in Figure 3-11. The PTO force and wave excitation force profiles for 2-DoF Pod-1 with Linear and Nonlinear MPC under linear hydrodynamic conditions are shown in Figure 3-12. The PTO velocity and displacement plots for 2-DoF Pod-1 with Linear and Nonlinear MPC under linear hydrodynamic conditions are shown in Figure 3-13.

The average and instantaneous electrical power output results under nonlinear hydrodynamics for 2-DoF Pod-1 with Linear and Nonlinear MPC are shown in Figure 3-14 and Figure 3-15, respectively. The comparison of average electrical PTO power output with NMPC for 1-DoF and 2-DoF Pod-1 is shown in Figure 3-16 under nonlinear hydrodynamic conditions.

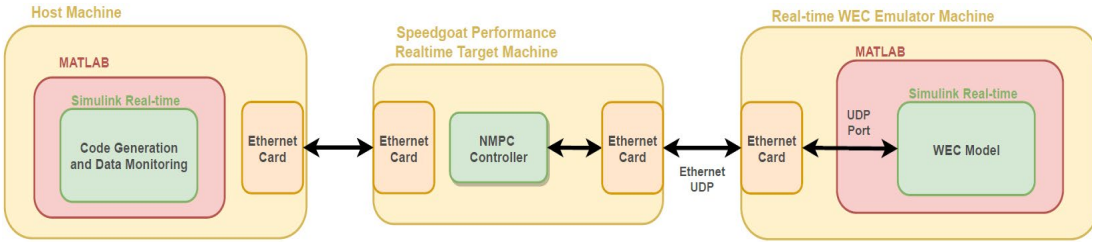

Figure 3-6 Schematic diagram of the test setup.

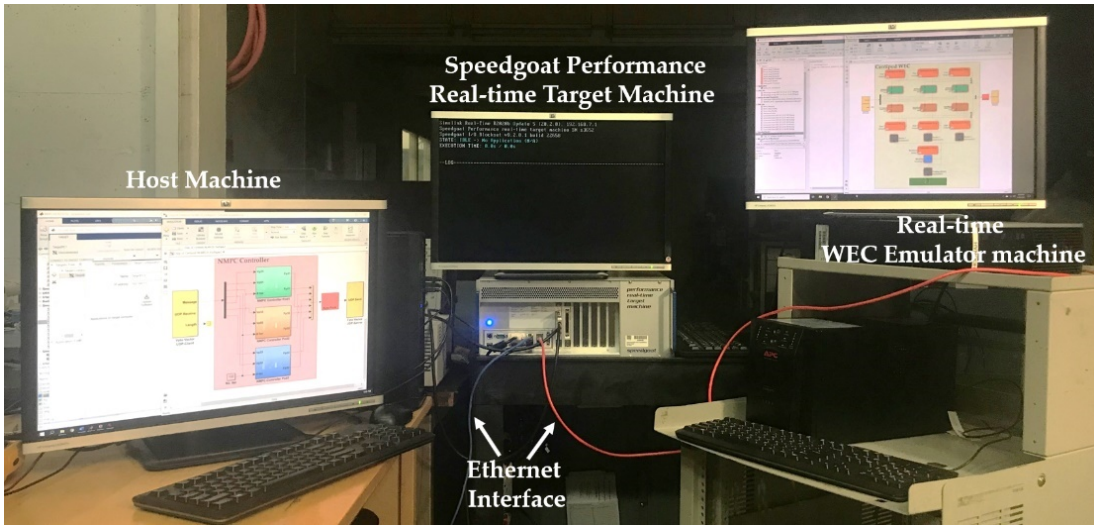

Figure 3-7 Hardware test setup.

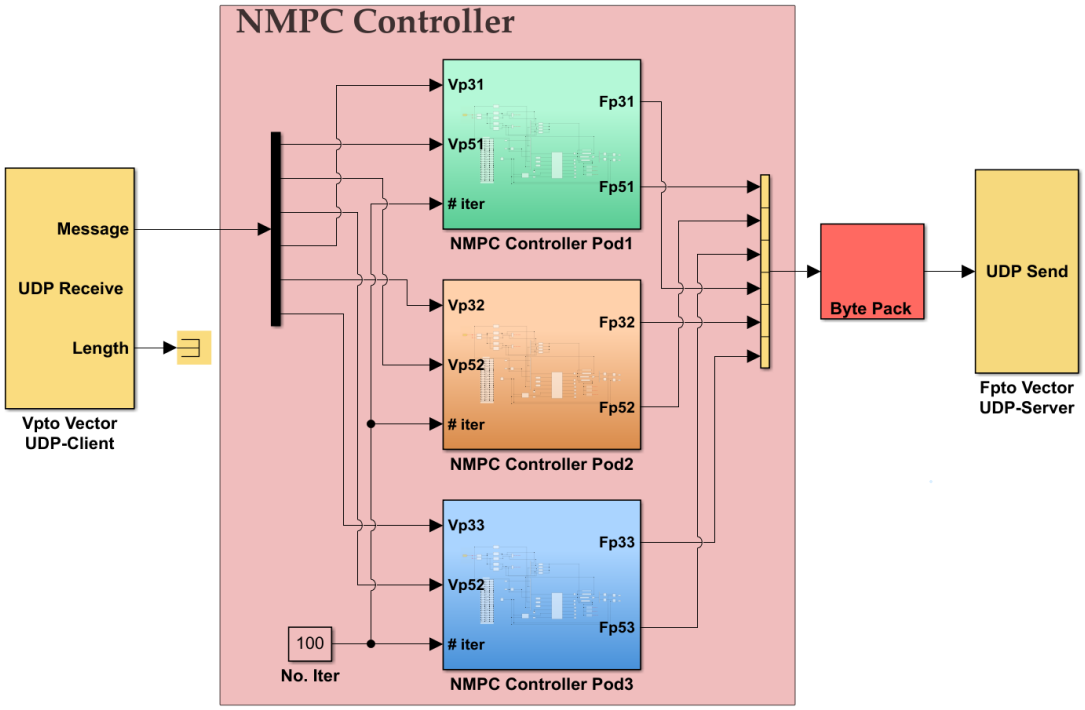

Figure 3-8 NMPC controller for 2-DoF 3-pod CENTIPOD WEC.

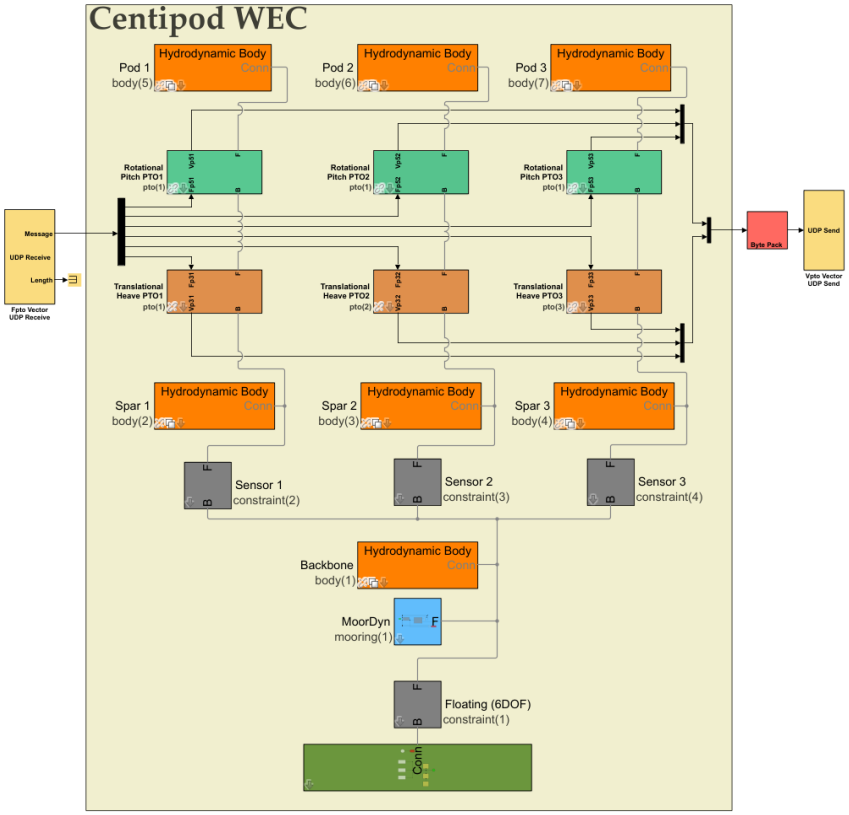

Figure 3-9 WEC-Sim model of Dehlsen's 2-DoF CENTIPOD device with heave and pitch PTOs for each pod.

Table 3-3 Sea states for WEC-Sim simulation.

WEC-Sim Simulation Parameter	Value
Significant Wave Height [m]	2.5
Peak Period [s]	8
Wave Spectrum Type	Pierson Moskowitz (PM)
Wave Class	Irregular

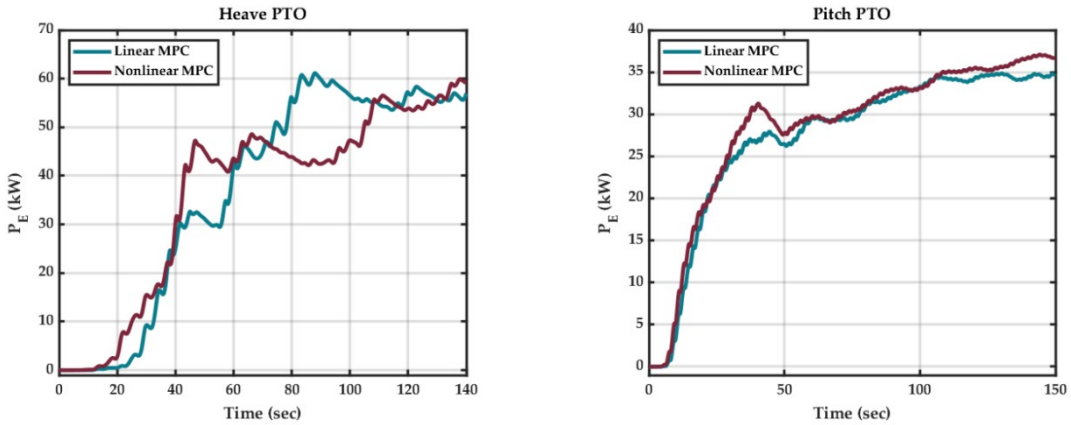

(a) (b)

Figure 3-10 Average electrical PTO power output for 2-DoF Pod-1 with Linear and Nonlinear MPC under linear hydrodynamic conditions in WEC-Sim and $|\boldsymbol{F_{pto}}| \leq \boldsymbol{400\ kN}$: (a) Pod-1 Heave PTO; (b) Pod-1 Pitch PTO.

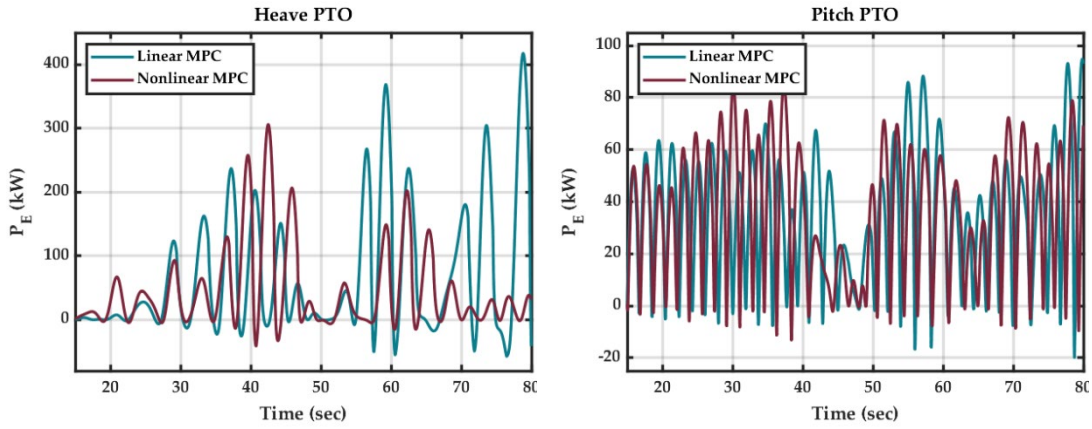

(a) (b)

Figure 3-11 Instantaneous electrical PTO power output for 2-DoF Pod-1 with Linear and Nonlinear MPC under linear hydrodynamic conditions in WEC-Sim and $|\boldsymbol{F_{pto}}| \leq \boldsymbol{400\ kN}$: (a) Pod-1 Heave PTO; (b) Pod-1 Pitch PTO.

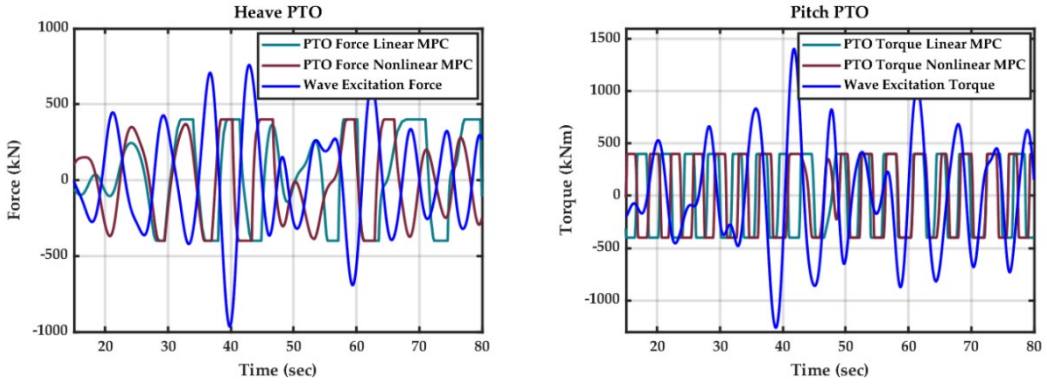

(a) (b)

Figure 3-12 The PTO force and wave excitation force profiles for 2-DoF Pod-1 with Linear and Nonlinear MPC under linear hydrodynamic conditions in WEC-Sim and $|\boldsymbol{F_{pto}}| \leq \boldsymbol{400\ kN}$: (a) Pod-1 Heave PTO; (b) Pod-1 Pitch PTO.

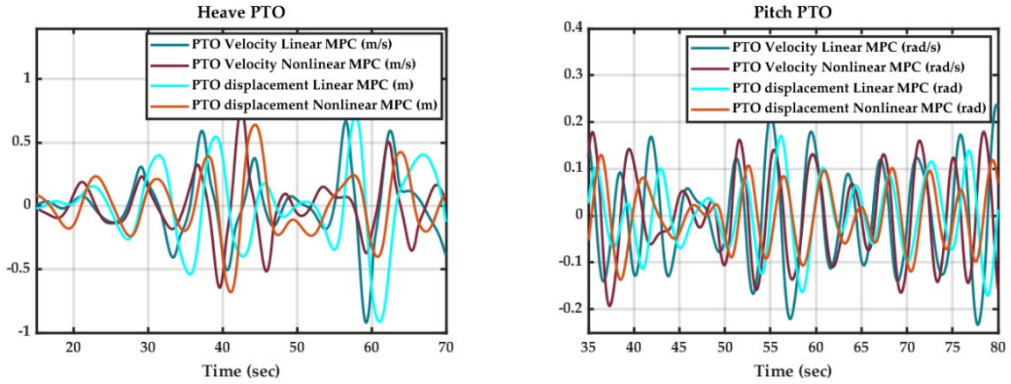

(a) (b)

Figure 3-13 The PTO velocity and displacement plots for 2-DoF Pod-1 with Linear and Nonlinear MPC under linear hydrodynamic conditions in WEC-Sim and $|\boldsymbol{F_{pto}}| \leq \boldsymbol{400\ kN}$: (a) Pod-1 Heave PTO; (b) Pod-1 Pitch PTO.

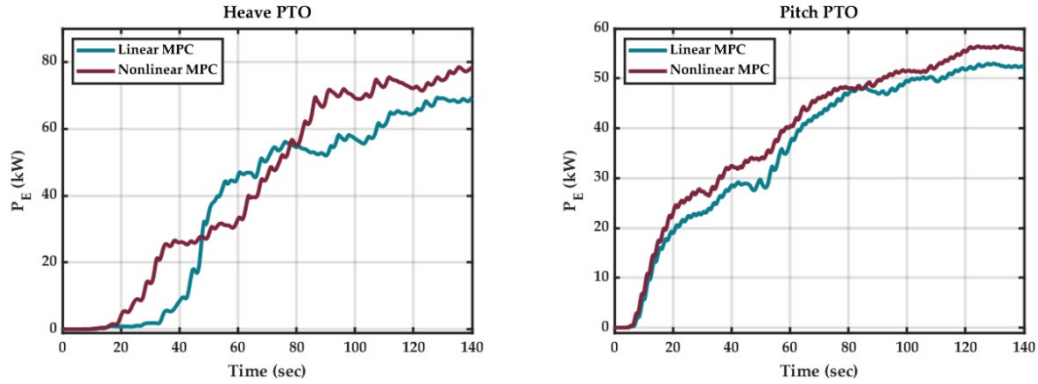

(a) (b)

Figure 3-14 Average electrical PTO power output for 2-DoF Pod-1 with Linear and Nonlinear MPC under Nonlinear hydrodynamic conditions in WEC-Sim and $|\boldsymbol{F_{pto}}| \leq \boldsymbol{400\ kN}$: (a) Pod-1 Heave PTO; (b) Pod-1 Pitch PTO.

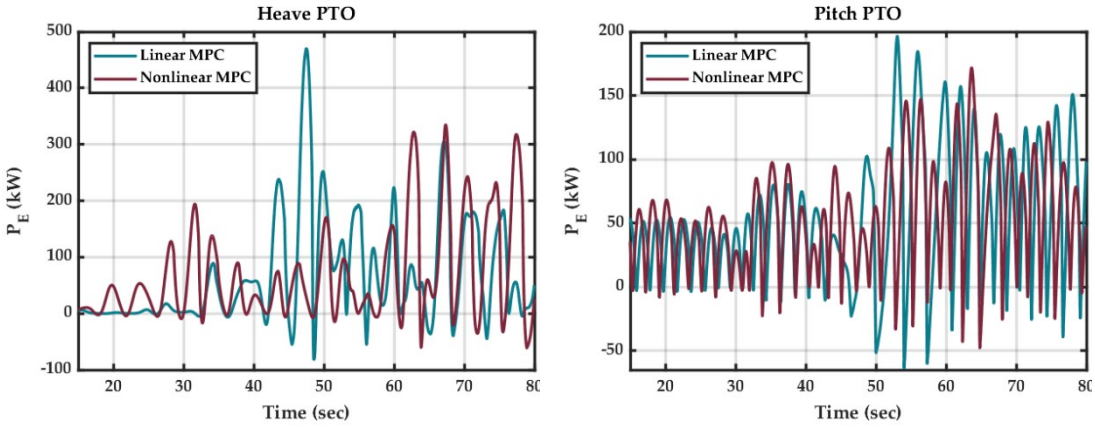

(a) (b)

Figure 3-15 Instantaneous electrical PTO power output for 2-DoF Pod-1 with Linear and Nonlinear MPC under Nonlinear hydrodynamic conditions in WEC-Sim and $|\boldsymbol{F_{pto}}| \leq \boldsymbol{400\ kN}$: (a) Pod-1 Heave PTO; (b) Pod-1 Pitch PTO.

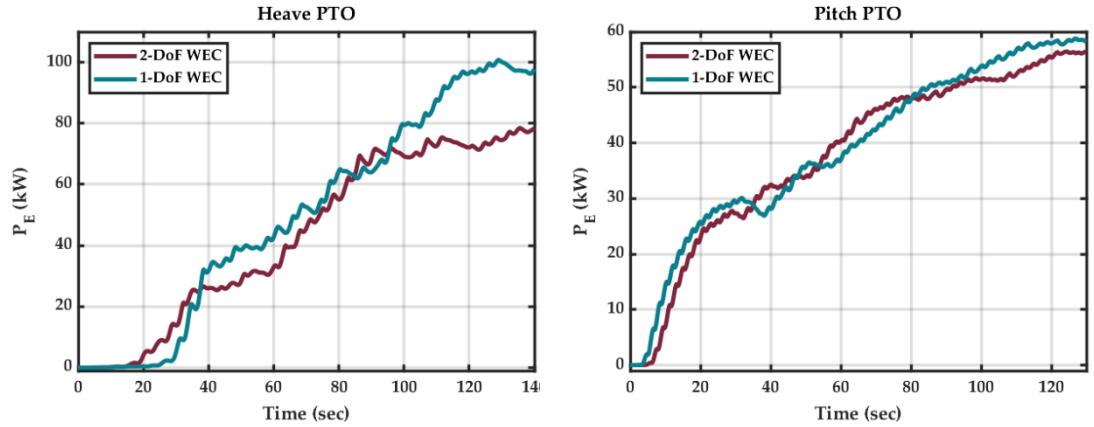

(a) (b)

Figure 3-16 Average electrical PTO power output for 1-DoF and 2-DoF Pod-1 with Nonlinear MPC under Nonlinear hydrodynamic conditions in WEC-Sim and $|\boldsymbol{F_{pto}}| \leq \boldsymbol{400\ kN}$: (a) Pod-1 Heave PTO; (b) Pod-1 Pitch PTO.

3.8 Discussion

The average electrical power output results in Figure 3-10 and Figure 3-14 are summarized in Table 3-4. NMPC shows a better performance in terms of increased power output when compared to Linear MPC. This increase in the output power becomes more prominent under nonlinear hydrodynamic conditions, which are not accounted for by the linear MPC. An overall 5% increase in power by NMPC compared

to linear MPC is obtained under linear hydrodynamic conditions. NMPC obtains an overall 5% increase in total power output by pod-1 than linear MPC under linear hydrodynamic conditions and 10.6% under nonlinear hydrodynamic conditions. The corresponding Task Execution Time (TET) stats for the real-time implementations of linear MPC and NMPC in Speedgoat real-time machine are given in Table 3-5. Given the controller step time of 0.1 sec, the increase in TET for NMPC compared to linear MPC is not very significant.

Table 3-4 Average electrical power output per PTO for 2-DoF Pod1 with linear MPC and NMPC.

	Average Electrical Power [kW]					
Control Algorithm	Linear Hydrodynamic Conditions			Nonlinear Hydrodynamic Conditions		
	Heave	Pitch	Total	Heave	Pitch	Total
Linear MPC	57	35	92	70	52	122
Nonlinear MPC	60	37	97	79	56	135

Table 3-5 Real-time timings stats for Linear MPC vs. Nonlinear MPC.

	Task Execution Time (TET) [sec]		
Control Algorithm	1-DoF Heave	1-DoF Pitch	2-DoF Heave and Pitch
Linear MPC	2.12×10^{-4}	2.67×10^{-4}	5.21×10^{-4}
Nonlinear MPC	3.05×10^{-4}	3.21×10^{-4}	6.14×10^{-4}

The average electrical power output results per PTO for 1-DoF and 2-DoF Pod1 with NMPC from Figure 3-16 are summarized in Table 3-6. In moving from 1-DoF

WEC to 2-DoF WEC, 35% increase in output power is obtained compared to heave only, and 129% increase compared to pitch only.

Table 3-6 Average electrical power output per PTO for 1-DoF and 2-DoF Pod1 with NMPC.

	Average Electrical Power [kW]		
	1-DoF WEC		2-DoF WEC
Axis	Heave	Pitch	Heave and Pitch
Heave	98	0	78
Pitch	0	58	55
Net Power	98	58	133

The locus of electrical PTO power for Linear MPC and NMPC under nonlinear hydrodynamic conditions in WEC-Sim, along with the electrical power cost functional surface from Figure 3-5, are shown in Figure 3-16.

The locus of electrical PTO power in Figure 3-16 traverses a trajectory on the cost manifolds and satisfies the cost objective. The cost index formulation in (15) includes a convexifying quadratic term of PTO current, making the resultant electrical PTO surface convex in Figure 3-5, and with a smooth PTO current profile, the close loop system tends to maintain a stable operation. If the QP problem formulated at a given sample interval is infeasible, the controller will not find a solution. This issue can be handled by monitoring the status of the QP solver during each sampling interval and selecting a suboptimal solution when the QP solver fails. An average of 35% processor load was observed per sampling interval during testing.

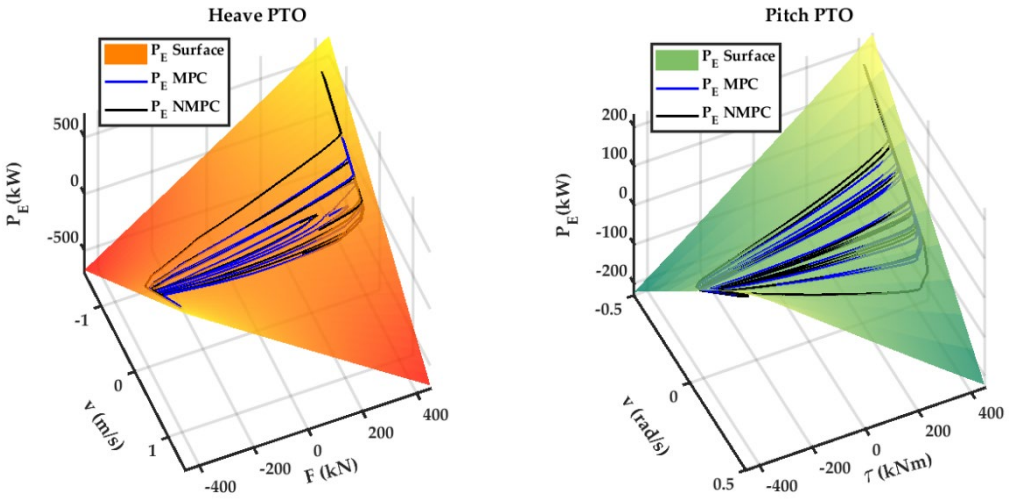

(a) (b)

Figure 3-17 The locus of electrical PTO power on the electrical power cost functional surface for Linear MPC and NMPC under nonlinear hydrodynamic conditions in WEC-Sim and $\left|\boldsymbol{F_{pto}}\right| \leq \mathbf{400}\ \boldsymbol{kN}$: (a) Pod-1 Heave PTO; (b) Pod-1 Pitch PTO.

3.9 Conclusions

This article presents a real-time implementation of NMPC for a nonlinear 2-DoF WEC based on Dehlsen Associates' CENTIPOD multi-pod WEC device, with non-ideal PTOs in the heave and pitch axes. The three pods of the WEC device are assumed identical, and a nonlinear state-space model of a single pod is developed. An NMPC controller is implemented for a 2-DoF WEC device with the cost functional based on a case study PTO model with a highly nonlinear PTO current-force characteristic. The results of the linear MPC are compared with NMPC for the sea states of interest (irregular waves with Pierson Moskowitz spectrum) under linear and nonlinear hydrodynamic conditions in WEC-Sim. The proposed methodology successfully maintained an overall feasible operation of the real-time NMPC problem in simulation as indicated by the status port of the NMPC QP-solver.

An average of 35% processor load was observed per sampling interval during testing. An overall 5% increase in total power output by a single pod is obtained by NMPC compared to linear MPC under linear hydrodynamic conditions and 10.6% under nonlinear hydrodynamic conditions. Moreover, a 35% increase in net output power is obtained by the 2-DoF WEC device compared to the 1-DoF heave only, and a 129% increase compared to the 1-DoF pitch only. While the result reflects only a single sea state, the improvement is likely to be reflected similarly in annual energy production (AEP). The AEP would have a substantive impact on the Levelized Cost of Energy (LCOE). The present work did not consider the cross-coupling between the three pods of the CENTIPOD device. The cross-coupling would be investigated in future work with anticipation of further increase the captured power for the sea conditions where the cross-coupling effect is no longer negligible.

3.10 References

1. Muetze, A.; Vining, J.G. Ocean Wave Energy Conversion - A Survey. In Proceedings of the Conference Record of the 2006 IEEE Industry Applications Conference Forty-First IAS Annual Meeting; October 2006; Vol. 3, pp. 1410–1417.
2. Richter, M.; Magana, M.E.; Sawodny, O.; Brekken, T.K.A. Nonlinear Model Predictive Control of a Point Absorber Wave Energy Converter. *IEEE Transactions on Sustainable Energy* **2013**, *4*, 118–126, doi:10.1109/TSTE.2012.2202929.
3. Haider, A.S.; Brekken, T.K.A.; McCall, A. A State-of-the-Art Strategy to Implement Nonlinear Model Predictive Controller with Non-Quadratic Piecewise Discontinuous Cost Index for Ocean Wave Energy Systems. In Proceedings of the 2020 IEEE Energy Conversion Congress and Exposition (ECCE); October 2020; pp. 1873–1878.
4. Brekken, T.K.A. On Model Predictive Control for a Point Absorber Wave Energy Converter. In Proceedings of the 2011 IEEE Trondheim PowerTech; June 2011; pp. 1–8.
5. Faedo, N.; Olaya, S.; Ringwood, J.V. Optimal Control, MPC and MPC-like Algorithms for Wave Energy Systems: An Overview. *IFAC Journal of Systems and Control* **2017**, *1*, 37–56, doi:10.1016/j.ifacsc.2017.07.001.
6. Zhong, Q.; Yeung, R.W. Model-Predictive Control Strategy for an Array of Wave-Energy Converters. *J. Marine. Sci. Appl.* **2019**, *18*, 26–37, doi:10.1007/s11804-019-00081-x.
7. Genest, R.; Ringwood, J.V. A Critical Comparison of Model-Predictive and Pseudospectral Control for Wave Energy Devices. *J. Ocean Eng. Mar. Energy* **2016**, *2*, 485–499, doi:10.1007/s40722-016-0058-2.
8. Li, G.; Belmont, M.R. Model Predictive Control of Sea Wave Energy Converters – Part I: A Convex Approach for the Case of a Single Device. *Renewable Energy* **2014**, *69*, 453–463, doi:10.1016/j.renene.2014.03.070.
9. Li, G.; Belmont, M.R. Model Predictive Control of Sea Wave Energy Converters – Part II: The Case of an Array of Devices. *Renewable Energy* **2014**, *68*, 540–549, doi:10.1016/j.renene.2014.02.028.
10. Genest, R.; Ringwood, J.V. A Critical Comparison of Model-Predictive and Pseudospectral Control for Wave Energy Devices. *J. Ocean Eng. Mar. Energy* **2016**, *2*, 485–499, doi:10.1007/s40722-016-0058-2.
11. Starrett, M.; So, R.; Brekken, T.K.A.; McCall, A. Increasing Power Capture from Multibody Wave Energy Conversion Systems Using Model Predictive Control. In Proceedings of the 2015 IEEE Conference on Technologies for Sustainability (SusTech); July 2015; pp. 20–26.
12. Falcão, A.F.O.; Henriques, J.C.C. Effect of Non-Ideal Power Take-off Efficiency on Performance of Single- and Two-Body Reactively Controlled Wave Energy Converters. *J. Ocean Eng. Mar. Energy* **2015**, *1*, 273–286, doi:10.1007/s40722-015-0023-5.
13. Davis, A.F.; Thomson, J.; Mundon, T.R.; Fabien, B.C. Modeling and Analysis of a Multi Degree of Freedom Point Absorber Wave Energy Converter.; American Society of Mechanical Engineers Digital Collection, October 1 2014.

14. Al Shami, E.; Wang, X.; Ji, X. A Study of the Effects of Increasing the Degrees of Freedom of a Point-Absorber Wave Energy Converter on Its Harvesting Performance. *Mechanical Systems and Signal Processing* **2019**, *133*, 106281, doi:10.1016/j.ymssp.2019.106281.
15. Strager, T.; Martin dit Neuville, A.; Fernández López, P.; Giorgio, G.; Mureşan, T.; Andersen, P.; Nielsen, K.M.; Pedersen, T.S.; Vidal Sánchez, E. Optimising Reactive Control in Non-Ideal Efficiency Wave Energy Converters.; American Society of Mechanical Engineers Digital Collection, October 1 2014.
16. Perdigão, J.; Sarmento, A. Overall-Efficiency Optimisation in OWC Devices. *Applied Ocean Research* **2003**, *25*, 157–166, doi:10.1016/j.apor.2003.09.002.
17. Tedeschi, E.; Carraro, M.; Molinas, M.; Mattavelli, P. Effect of Control Strategies and Power Take-Off Efficiency on the Power Capture From Sea Waves. *IEEE Transactions on Energy Conversion* **2011**, *26*, 1088–1098, doi:10.1109/TEC.2011.2164798.
18. Jia, Y.; Meng, K.; Dong, L.; Liu, T.; Sun, C.; Dong, Z.Y. Economic Model Predictive Control of a Point Absorber Wave Energy Converter. *IEEE Transactions on Sustainable Energy* **2021**, *12*, 578–586, doi:10.1109/TSTE.2020.3012755.
19. Ellis, M.; Durand, H.; Christofides, P.D. A Tutorial Review of Economic Model Predictive Control Methods. *Journal of Process Control* **2014**, *24*, 1156–1178, doi:10.1016/j.jprocont.2014.03.010.
20. Rawlings, J.B.; Angeli, D.; Bates, C.N. Fundamentals of Economic Model Predictive Control. In Proceedings of the 2012 IEEE 51st IEEE Conference on Decision and Control (CDC); December 2012; pp. 3851–3861.
21. Houska, B.; Ferreau, H.J.; Diehl, M. An Auto-Generated Real-Time Iteration Algorithm for Nonlinear MPC in the Microsecond Range. *Automatica* **2011**, *47*, 2279–2285, doi:10.1016/j.automatica.2011.08.020.
22. Houska, B.; Ferreau, H.J.; Diehl, M. ACADO Toolkit—An Open-Source Framework for Automatic Control and Dynamic Optimization. *Optimal Control Applications and Methods* **2011**, *32*, 298–312, doi:https://doi.org/10.1002/oca.939.
23. Abdelkhalik, O.; Zou, S.; Robinett, R.D.; Bacelli, G.; Wilson, D.G.; Coe, R.; Korde, U. Multiresonant Feedback Control of a Three-Degree-of-Freedom Wave Energy Converter. *IEEE Transactions on Sustainable Energy* **2017**, *8*, 1518–1527, doi:10.1109/TSTE.2017.2692647.
24. Frequency- and Time-Domain Analysis of a Multi-Degree-of-Freedom Point Absorber Wave Energy Converter - Yizhi Ye, Weidong Chen, 2017 Available online: https://journals.sagepub.com/doi/full/10.1177/1687814017722081 (accessed on 20 July 2021).
25. Coe, R.G.; Bull, D.L. Nonlinear Time-Domain Performance Model for a Wave Energy Converter in Three Dimensions. In Proceedings of the 2014 Oceans - St. John's; September 2014; pp. 1–10.
26. Huang, S.; Shi, H.; Dong, X. Capture Performance of A Multi-Freedom Wave Energy Converter with Different Power Take-off Systems. *China Ocean Eng* **2019**, *33*, 288–296, doi:10.1007/s13344-019-0028-2.
27. Hillis, A.J.; Whitlam, C.; Brask, A.; Chapman, J.; Plummer, A.R. Active Control for Multi-Degree-of-Freedom Wave Energy Converters with Load Limiting. *Renewable Energy* **2020**, *159*, 1177–1187, doi:10.1016/j.renene.2020.05.073.

28. Li, G. Nonlinear Model Predictive Control of a Wave Energy Converter Based on Differential Flatness Parameterisation. *International Journal of Control* **2017**, *90*, 68–77, doi:10.1080/00207179.2015.1088173.
29. WEC-Sim (Wave Energy Converter SIMulator) — WEC-Sim Documentation Available online: https://wec-sim.github.io/WEC-Sim/ (accessed on 27 March 2021).
30. van Rij, J.; Yu, Y.-H.; McCall, A.; Coe, R.G. Extreme Load Computational Fluid Dynamics Analysis and Verification for a Multibody Wave Energy Converter.; American Society of Mechanical Engineers Digital Collection, November 11 2019.
31. Haider, A.S.; Brekken, T.K.A.; McCall, A. Application of Real-Time Nonlinear Model Predictive Control for Wave Energy Conversion. *IET Renewable Power Generation n/a*, doi:10.1049/rpg2.12257.
32. Speedgoat - The Quickest Path to Real-Time Simulation and Testing Available online: https://www.speedgoat.com/ (accessed on 23 February 2021).
33. Ecomerit Technologies Available online: http://www.ecomerittech.com/centipod.php (accessed on 14 August 2021).
34. Garcia-Rosa, P.B.; Bacelli, G.; Ringwood, J.V. Control-Informed Optimal Array Layout for Wave Farms. *IEEE Transactions on Sustainable Energy* **2015**, *6*, 575–582, doi:10.1109/TSTE.2015.2394750.
35. Wamit, Inc. - The State of the Art in Wave Interaction Analysis Available online: https://www.wamit.com/ (accessed on 28 March 2021).
36. Ringwood, J.V. Wave Energy Control: Status and Perspectives 2020 □□This Paper Is Based upon Work Supported by Science Foundation Ireland under Grant No. 13/IA/1886 and Grant No. 12/RC/2302 for the Marine Renewable Ireland (MaREI) Centre. *IFAC-PapersOnLine* **2020**, *53*, 12271–12282, doi:10.1016/j.ifacol.2020.12.1162.
37. ACADOToolkitUser's Manual. 116.

4 Manuscript 3:

On Real-time Hybrid Testing of Ocean Wave Energy Conversion Systems: An Experimental Study

Ali S. Haider, Ted K.A. Brekken

IEEE Open Journal of Industry Applications

(In submission)

25 August 2021

4.1 Abstract

The growing wave energy sector requires an efficient and flexible testing process at the development phase of wave energy systems. Real-time hybrid testing is a promising technique for the accelerated testing of wave energy conversion systems. This article presents an experimental study on developing a hybrid testing platform for wave energy systems at the Wallace Energy System and Renewables Facility (WESRF) at Oregon State University. The wave energy conversion system is broken down into numeric (i.e., virtual) and physical (i.e., hardware) components. The numeric component involves software components such as the control algorithm for Wave Energy Converter (WEC) and controller for the power electronic converters and numerical models for the WEC device hydrodynamics. The hardware involves an ocean wave emulator testbed, Power Take-Off (PTO) mechanism, power electronics, and instrumentation. The numeric components are implemented in a real-time target machine, which is interfaced with the experimental system. A case study implementation of Nonlinear Model Predictive Control (NMPC) is presented for a single degree of freedom heaving nonlinear WEC model with a Permanent Magnet Synchronous Generator (PMSG) as a PTO system. A Field-Oriented Control (FOC) algorithm controls the PMSG-PTO generation using a three-phase Integrated Intelligent Power (IIP) module converter. A demonstration of the proposed hybrid testing setup is provided.

4.2 Introduction

Renewable energy technologies present a sustainable, low-carbon solution to growing global energy demands. The ocean provides a potential for an untapped energy

resource for the world's increasing appetite for energy, with its low environmental effect and greater energy density [1], [2]. Ocean wave energy is converted to mechanical energy by Wave Energy Converter (WEC) devices. Among WEC devices, point absorbers (floating buoys) are promising solutions to capture wave energy [3], [4]. Conversion of mechanical energy to electrical energy requires Power Take-Off (PTO) mechanisms. The control strategy of PTO systems needs to ensure some energy conversion advantage within the system physical and operational constraints to ensure the economical operation of the wave energy conversion system. Therefore, optimal control of the PTO system is vital to the overall profitable operation of the WEC system. Among various control techniques for WEC are reactive control and latching [5], spectral methods, and pseudospectral techniques [6], [7]. Optimal control strategies have been explored in detail in the literature [2], [8].

Model Predictive Control (MPC) is an extensively studied controller strategy in this context [9]–[12]. MPC is an online optimization method that maximizes a given cost index while respecting system constraints. Typically, the optimization objective of the MPC problem for WEC is to maximize the power capture by the PTO mechanism. However, other alternative formulations, such as Economic MPC [13], [14], are also explored to maximize economic operation metrics. Since MPC is a model-based control scheme, the system dynamics may be linear or include nonlinear effects, such as fluid viscous drag or mooring forces. Nonlinear MPC (NMPC) formulations have gained popularity because the WEC devices operate in non-ideal environments where nonlinear effects cannot be neglected. NMPC has also been investigated for WECs in literature. For example, an NMPC formulation based on differential flatness is

presented in [15]. The nonlinear effects of mooring lines are presented in [9], and the effects of nonlinear fluid viscous drag are investigated in [16].

Moreover, the PTO mechanism is typically considered ideal. However, their reduced efficiency does negatively affect the optimal operation of the WEC system [17]–[19]. Some recent studies also consider the nonlinear PTO machine characteristics [20].

A more efficient and flexible testing process is needed to develop wave energy converter systems and the PTO mechanism for the growing wave energy sector [21]. The real-time hybrid testing method is a promising technique for the accelerated testing of WEC and PTO systems at their development phase. It involves breaking down the system into numerical and physical components and running the integrated hardware-software set up in real-time to access and evaluate the overall system performance [22]. Such accelerated testing techniques save product development costs, have been very successful in the automotive industry [23], and share some structural ideas with hardware-in-the-loop testing. These techniques are also gaining popularity in the WEC development sector [24]. This study aims to develop a hybrid testing platform at Wallace Energy Systems and Renewables Facility (WESRF) at the Oregon State University [25]. This experimental study involves breaking down a case-study point absorber type WEC testing into numerical (i.e., virtual) models and physical (i.e., hardware) systems and running them in real-time to evaluate control techniques under numerous sea states. The hardware parts involve a scaled nonlinear PTO system coupled with a Linear Testbed (LTB) wave simulator, power electronics converters, electrical load, and sensors and instrumentation. The numeric component consists of a

nonlinear model of a heaving WEC, the NMPC algorithm, and power electronics control. The numeric parts are implemented in real-time, which is interfaced with the various hardware components. The hybrid testing experiments are performed, and results of the successful performance of the hybrid platform are presented.

4.3 Time Domain Model of WEC

The WEC device is a full-scale version of the Dehlsen Associates, LLC multi-pod CENTIPOD [26], [27]. A 1:35-scale version of the device is shown in Figure 4-1. This WEC device has three floating pods and three spars fixed to a single backbone structure. The backbone is anchored using mooring lines. In this work, a single pod from Figure 4-1 is selected for hybrid testing. We will follow the subscript notation of WEC-Sim Toolbox [28] for the degrees of freedom for WEC, in which the integers from 1, 2,…, 6 correspond to surge, sway, heave, roll, pitch, and yaw, respectively. Other notations and symbols for WEC modeling are given in Table 4-1.

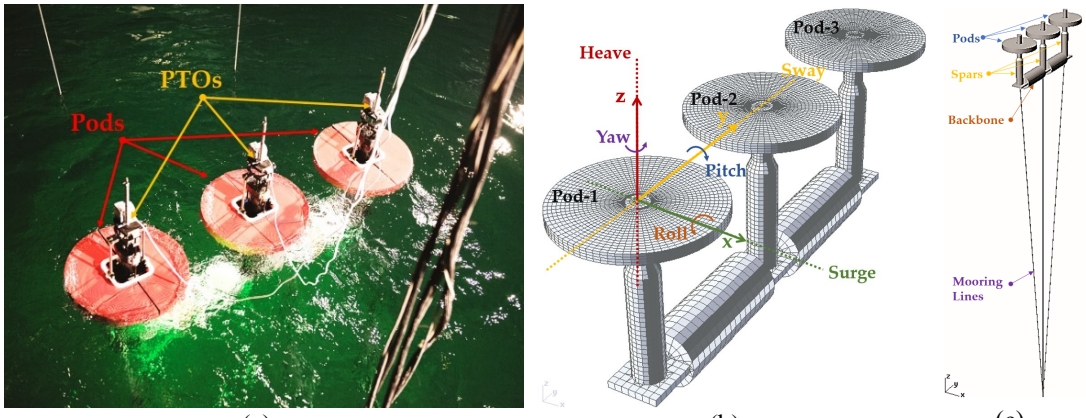

(a) (b) (c)

Figure 4-1 Image of the Dehlsen Associates, LLC, 1:35-scale CENTIPOD WEC: (a) WEC Model; (b) baseline configuration; (b) model with mooring lines.

Table 4-1 Notations and symbols for WEC modelling.

Variable	Description
v_i	Velocity (Linear or Angular) in i^{th} DoF
x_i	Displacement (Linear or Angular) in i^{th} DoF
ξ_i	Intermediate State variables for radiation force State-Space approximation
$F_{r,pq}$	Radiation force in p^{th} DoF due to velocity in q^{th} DoF
$F_{hs,i}$	Hydrostatic force in i^{th} DoF
$F_{v,i}$	Viscous drag force in i^{th}DoF
$F_{e,i}$	Wave excitation force in i^{th}DoF
$F_{p,i}$	PTO force in i^{th}DoF
m	Mass of the float
$A_{pq}(\infty)$	Added mass at the infinite frequency in p^{th} DoF due to acceleration in q^{th} DoF
C_i	The hydrostatic restoring coefficient in i^{th} DoF
$C_{vd,i}$	Viscous drag coefficient in i^{th} DoF
A_{qp}	Frequency-dependent added mass in p^{th} DoF due to acceleration in q^{th} DoF
B_{qp}	Frequency-dependent damping in p^{th} DoF due to velocity in q^{th} DoF
K_{pq}	Radiation force impulse response without infinite frequency added mass
Z_{qp}	WEC Intrinsic impedance response in p^{th} DoF due to velocity in q^{th} DoF
a_i	Polynomial coefficients
$c_{i,j}$	Polynomial coefficients for cost functional
$I_{p,i}$	i^{th} PTO current
η_{Conv}	PTO converter efficiency
K_{Cu}	PTO generator copper loss constant
R_s	PTO generator winding resistance

4.3.1 Heave Dynamics of WEC

The Cummins equation for the heave dynamics of a point absorber pod is given by,

$$\begin{aligned}\big(m + A_{33}(\infty)\big)\dot{v}_3(t) \\ = -F_{r,33}(t) - F_{hs,3}(t) - F_{v,3}(t) - F_{p,3}(t) + F_{e,3}(t),\end{aligned} \tag{1}$$

The hydrostatic, viscous damping, and radiation force terms in (1) are given by,

$$F_{r,33}(t) = \int_{-\infty}^{t} K_{33}(t-\tau)v_3 d\tau, \tag{2}$$

$$F_{hs,3}(t) = C_3 x_3, \tag{3}$$

$$F_{v,3}(t) = C_{d,3} v_3 |v_3|. \tag{4}$$

A transfer function expression can approximate the convolution integral term in (2),

$$F_{r,33}(t) = \int_{-\infty}^{t} K_{33}(t-\tau)v_3 d\tau \Leftrightarrow F_{r,33}(j\omega) = Z_{33}(j\omega)V_3(j\omega), \tag{5}$$

Using the device data from WAMIT [29], we can approximate the intrinsic impedance $Z_{pq}(j\omega)$ in (5) by a second order transfer function using System Identification techniques,

$$\begin{aligned}Z_{33}(j\omega) &= \big[j\omega\big(A_{33}(j\omega) - A_{33}(\infty)\big) + B_{33}(j\omega)\big] \\ &\approx \frac{\alpha_{33,1}s + \alpha_{33,0}}{s^2 + \beta_{33,1}s + \beta_{33,0}}\bigg|_{s=j\omega},\end{aligned} \tag{6}$$

The transfer function expression in (6) can be converted to the State-Space expressions in the Observer-Canonical form for the radiation force,

$$\begin{bmatrix}\dot{\xi}_1(t) \\ \dot{\xi}_2(t)\end{bmatrix} = \begin{bmatrix}0 & 1 \\ a_1 & a_2\end{bmatrix}\begin{bmatrix}\xi_1(t) \\ \xi_2(t)\end{bmatrix} + \begin{bmatrix}b_1 \\ b_2\end{bmatrix} v_3(t), \tag{7}$$

$$y_{33}(t) = [1 \quad 0]\begin{bmatrix}\xi_1(t)\\ \xi_2(t)\end{bmatrix} = \xi_1(t) \approx F_{r,33}(t). \tag{8}$$

Defining a state vector for the WEC as

$$\mathbf{X} = [v_3 \quad z_3 \quad F_{r,33} \quad \xi_2]^T, \tag{9}$$

with $M_{33} = \left(m + A_{33}(\infty)\right)$, and using (3), (4), (7), and (8) in (1), we get the following nonlinear state-space model for the WEC,

$$\begin{aligned}\dot{\mathbf{X}} &= \mathbf{g}(\mathbf{X}, \mathbf{U})\\ &= \begin{bmatrix}\frac{-C_3}{M_{33}}x_2 - \frac{1}{M_{33}}F_{r,33} - \frac{C_{d,3}}{M_{33}}v_3|v_3| - \frac{1}{M_{33}}F_{p,3} + \frac{1}{M_{33}}F_{e,3}\\ v_3\\ b_1 v_3 + \xi_2\\ b_1 v_3 + a_1 F_{r,33} + a_2\xi_2\end{bmatrix}.\end{aligned} \tag{10}$$

4.3.2 Nonquadratic WEC-PTO Model

For a given PTO generator, the electrical PTO power cost functional to be maximized, including the electrical losses, is given by,

$$\begin{aligned}\max_{F_{p,3}} P_{E,3} &= \eta_{Conv}\left(P_{Mechanical,3} - P_{Loss,3}\right)\\ &= \eta_{Conv}\left(F_{p,3}v_3 - K_{Cu}\left[I_{p,3}(F_{p,3})\right]^2 R_\Omega\right),\end{aligned} \tag{11}$$

The case study scenario is taken from McCleer Power's Linear PTO generator [20] with the PTO generator force-current characteristics given by Figure 4-2(a). We can approximate the experimental data in Figure 4-2 is approximated by a smooth third-order polynomial curve fit between the PTO current and the PTO force,

$$I_{p,3}(F_{p,3}) = a_{3,3}F_{p,3}^3 + a_{2,3}F_{p,3}^2 + a_{1,3}F_{p,3} + a_{0,3}, \tag{12}$$

Putting (12) in (11), we get,

$$P_{E,3} = c_{0,3}F_{p,3}v_3 - (c_{1,3}F_{p,3}^6 + c_{2,3}F_{p,3}^5 + c_{3,3}F_{p,3}^4 + c_{4,3}F_{p,3}^3 + c_{5,3}F_{p,3}^2 + c_{6,3}F_{p,3} + c_{7,3}), \quad (13)$$

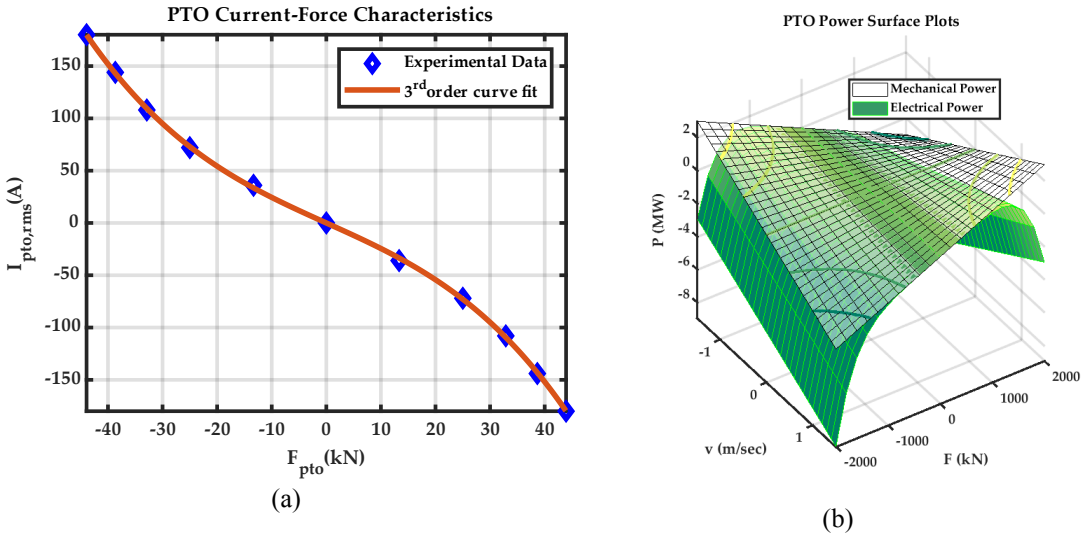

(a) (b)

Figure 4-2 PTO generator force-current characteristics: (a) Polynomial curve fitting to the PTO force-current experimental data for a PTO generator; (b) Mechanical and electrical PTO power surface plot in PTO velocity-force plane.

The mechanical and electrical PTO surface plots from (11) are shown in Figure 2(b). The mechanical power surface is non-convex, while the electrical power surface is convex due to the quadratic convexifying power loss term in (11).

4.4 Implementation of NMPC for WEC

MPC is a model-based online optimal control solution, and a given NMPC problem optimizes a manipulated variable $\mathrm{u}(t)$ to maximize some cost functional $\mathrm{P}(\cdot)$ while respecting the system's physical constraints. A special class of NMPC problem has been formulated in [16,20], in which the cost functional takes on a nonlinear piecewise polynomial form. Considering the case of finite-horizon optimization control, we can mathematically describe the NMPC problem of such a class as,

$$\underset{\mathbf{u}(t)}{maximize}\ \mathbf{P}\left[t, \dot{\mathbf{X}}(t), \mathbf{X}(t), \mathbf{U}(t), \mathbf{p}(t)\right] \tag{14}$$

$$\text{Where: } \mathbf{P}(\cdot) = \begin{cases} P_1(\cdot) + \rho_{N,1}(\cdot), & q_k(t) < R_1 \\ P_2(\cdot) + \rho_{N,2}(\cdot), & R_1 \le q_k(t) \le R_2 \\ \vdots & \vdots \\ P_j(\cdot) + \rho_{N,j}(\cdot), & R_{j-1} \le q_k(t) \le R_j \end{cases}, \tag{15}$$

subject to,

$$\text{Dynamic Constraints: } \mathbf{0} = \mathbf{f}\left(t, \dot{\mathbf{X}}(t), \mathbf{X}(t), \mathbf{U}(t), \mathbf{d}(t), \mathbf{p}(t), N\right), \tag{16}$$

$$\text{Boundary Constraint Function: } \mathbf{0} = \mathbf{r}(N, \mathbf{X}(0), \mathbf{U}(0), \mathbf{X}(N), \mathbf{U}(N), \mathbf{p}), \tag{17}$$

$$\text{Path Constraints Function: } 0 \ge \mathbf{s}(t, \mathbf{X}(t), \mathbf{U}(t), \mathbf{p}(t)). \tag{18}$$

The description of various variables and constants in the control formulation (14) through (18) is given in Table 4-2.

Table 4-2 Symbols and notations for NMPC formulation.

Variable	Description
N	Prediction horizon
X	State vector
$\rho_{N,i}$	Finite horizon terminal cost penalty or Mayer terms
$P_i(\cdot)$	Some Nonlinear functions or Lagrange terms
p	A column vector of time-varying parameters
U	PTO Force manipulated variable vector, $F_p(N)$
d	Excitation force disturbance vector, F_e (N)
$q_k(t)$	Cost functional scheduling variable
R_i	Some real numbers, such that $R_{k+1} > R_k$

The wave excitation force is an unmeasured disturbance and is estimated internally by the controller. For the NMPC problem for WEC, cost objective (14) takes the form of (11).

4.4.1 Prediction Model for NMPC

The NMPC algorithm optimizes a cost functional given by (11) that involves PTO current, a function of PTO force. So, we have developed an augmented model for WEC to be used as a prediction model for the NMPC optimization problem. Defining the augmented state vector as

$$\mathbf{X_a} = [v_3 \quad z_3 \quad \xi_1 \quad \xi_2 \quad F_{p,3} \quad I_{p,3}]^T, \tag{19}$$

Using (10) and (12) along with the state definition (19), we get the following augmented model for the WEC for NMPC prediction, with $u_a = \dot{F}_{p,3}$ as the manipulated variable,

$$\begin{aligned}\dot{\mathbf{X}}_\mathbf{a} &= \mathbf{g}(\mathbf{X_a}, \mathbf{U_a}) \\ &= \begin{bmatrix} \frac{-C_3}{M_{33}} z_3 - \frac{1}{M_{33}} F_{r,33} - \frac{C_{d,3}}{M_{33}} v_3|v_3| - \frac{1}{M_{33}} F_{p,3} + \frac{1}{M_{33}} F_{e,3} \\ v_3 \\ b_1 v_3 + \xi_2 \\ b_1 v_3 + a_1 \xi_1 + a_2 \xi_2 \\ \dot{F}_{p,3} \\ 3a_{3,3} F_{p,3}^2 \dot{F}_{p,3} + 2a_{2,3} F_{p,3} \dot{F}_{p,3} + a_{1,3} \dot{F}_{p,3} \end{bmatrix}.\end{aligned} \tag{20}$$

4.4.2 PMSG Control Strategy

A Permanent Magnetic Synchronous Generator (PMSG) is used as a PTO generator. PMSG is modeled in the qd-frame. The voltage equations for the generator in dq-frame are given by,

$$v_d = R_s i_d + L_q \frac{di_d}{dt} - \omega_e L_q i_q \,, \tag{21}$$

$$v_q = R_s i_q + L_q \frac{di_q}{dt} + \omega_e \Psi_{PM} + \omega_e L_d i_d. \tag{22}$$

where ω_e is the electrical velocity, Ψ_{PM} is the permanent magnet flux linkage, and the subscripted d and q represent the direct and quadrature axis, respectively. Values of various parameters for the PMSG are summarized in Table 4-3. The electro-mechanical torque developed by the generator is given by,

$$\tau_{em} = \frac{3}{2} P\big(\Psi_{PM} i_q - \big(L_d - L_q\big) i_d i_q\big), \tag{23}$$

Since we use surface-mounted PMSG, the d-axis and q-axis inductances are equal, and the dq-axis cross-coupling term in (23) vanishes. With a physical scaling parameter K_s, the PTO force relation can be obtained from (23) as,

$$F_{pto,PMSG} = K_s \tau_{em} = \frac{3}{2} K_s P \Psi_{PM} i_q, \tag{24}$$

The d-axis current of the PTO PMSG is controlled using standard Field Oriented Control (FOC) [30]. The stator phase currents are converted to dq-axis currents using Park transformation. The electrical angle θ_e and the electrical angular velocity ω_e are measured using a three-phase sinusoidal Phase Looked Loop (PLL). The commanded value of the d-axis current is zero, and the reference value of the q-axis current is calculated from (24). The PI controllers are used to convert current errors into dq-axis reference voltages. The DC link voltage is measured, and the dq-axis reference voltages are converted to PWM for the three-phase Voltage Source Inverter (VSI) using

the Space Vector Modulation (SVM) technique. The schematic diagram for the FOC control method is shown in Table 4-3.

Table 4-3 PMSG PTO generator parameters.

Variable	Description	Value
P_r	Rated Power	$6000\ W$
V_r	Rated Voltage	$330\ V$
I_r	Rated Current	$15.7\ A$
ω_r	Rated Speed	$220\ RPM$
τ_r	Rated Torque	$347\ N.m$
P	Pole Pairs	12
Ψ_{PM}	Permanent-Magnet flux linkage	$1.194\ Wb$
τ_c	Cogging Torque	$3\ N.m$
J	Rotor Inertia	$0.245\ Kg.m^2$
R_s	Stator Resistance	$1.42\ \Omega$
L_d, L_q	d-axis Inductance	$30.50\ mH$

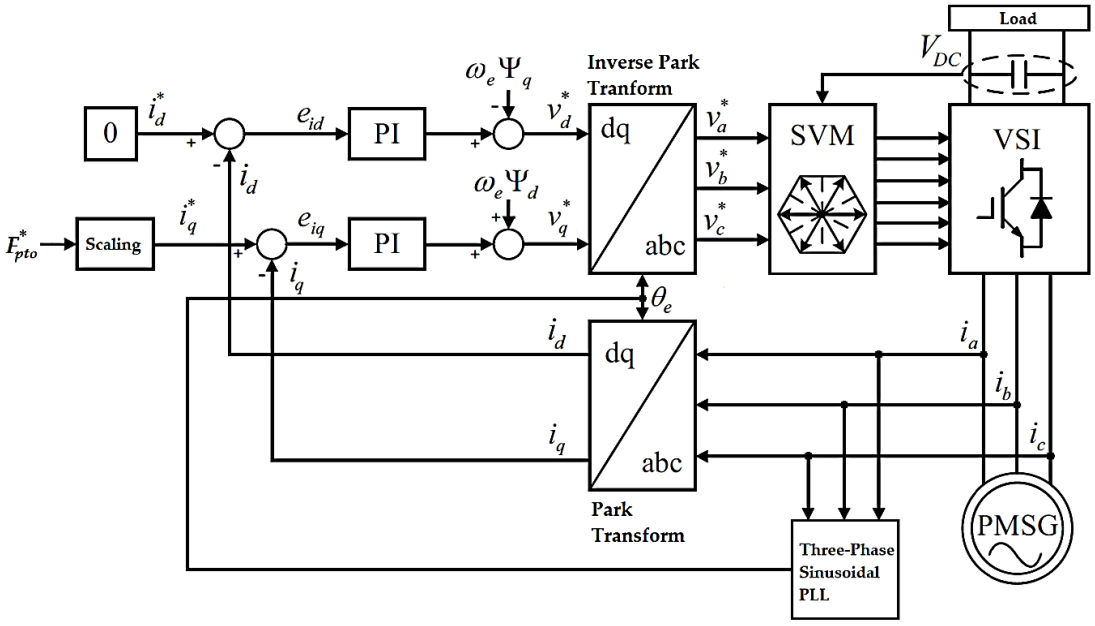

Figure 4-3 Schematic Diagram of Field-Oriented Control (FOC) for the PMSG-PTO generator.

4.5 Hybrid Testing Scheme of NMPC with PTO Hardware-in-Loop

The hybrid testing involves breaking down the system into physical (i.e., hardware) and numeric (i.e., software) parts, as shown in Figure 4-4.

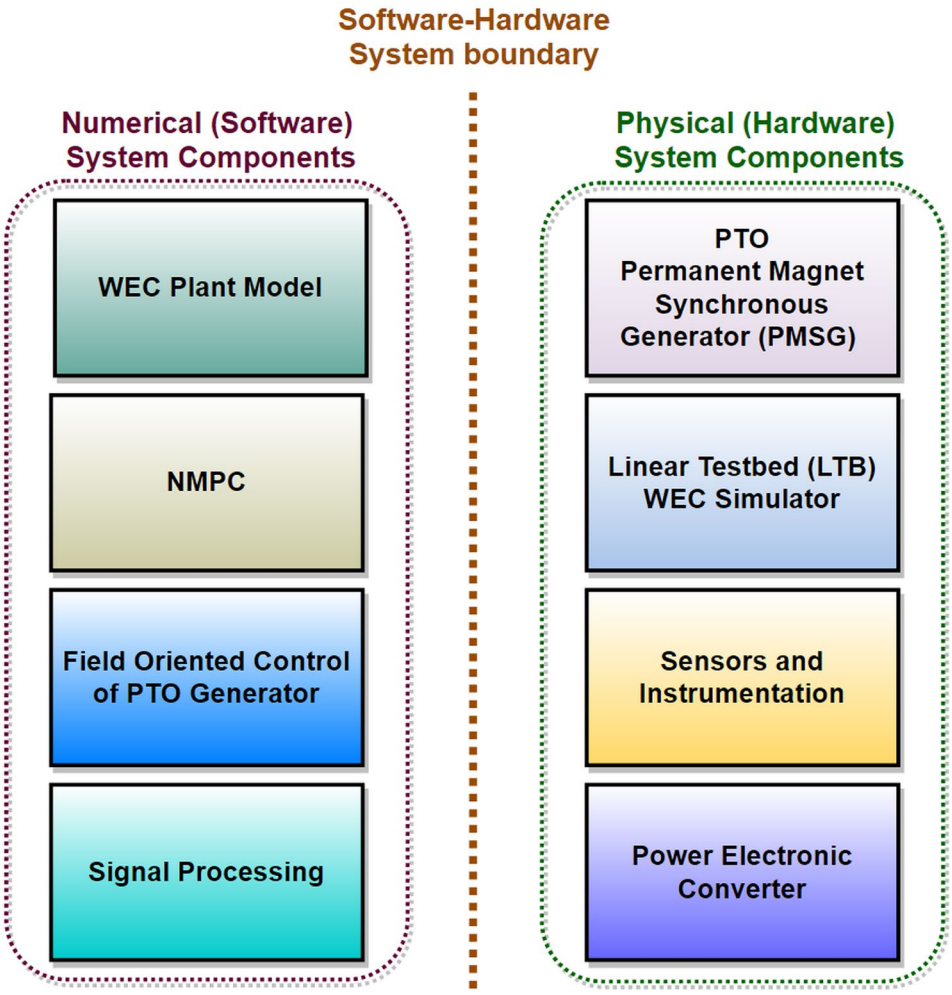

Figure 4-4 Hardware-Software system breakdown for the hybrid testing platform.

The hybrid testing experimental setup is shown in Figure 4-5. The control algorithm for WEC, i.e., NMPC, and WEC plant dynamics, are implemented in the Speedgoat Performance real-time target machine [32], model-109100 with Intel Core i3 3.3 GHz, two cores, and 2048MB DDR3 RAM. The heave displacement of WEC is commanded to Mundt's Linear Testbed (LTB) wave simulator machine [31] at the Wallace Energy Systems and Renewables Facility (WESRF) at Oregon State

University. The heaving cart of LTB is tethered to the winch of a PTO generation mechanism, which is a PMSG coupled to a torsional restoring spring. NMPC acts as a high-level supervisory controller, solving its online optimization problem and issuing an optimal PTO force command at its sample time of 0.1 sec. The PTO force command is translated into q-axis current reference using (24). The PMSG-PTO generator is controlled using the q-axis current of its stator, using the low-level Field Oriented Control programmed in the Speedgoat machine with a sample time of 0.001 sec. We have used Semikron's SKiiP-603-GD123-3DUL-V3 three-phase IGBT Integrated Intelligent Power (IIP) modular bridge rectifier [32] as a Voltage Source Inverter (VSI) in Figure 4-3. The actual PTO force output of PMSG is feedback to the NMPC. The WEC plant in Speedgoat receives the input PTO force from the loadcells on the LTB cart that monitor the tether tension in real-time. The schematic diagram of the hybrid testing scheme is shown in Figure 4-6.

The Simulink model for code generation and deployment in the Speedgoat target machine for hybrid testing is shown in Figure 4-7. The WEC model receives a preprogrammed real-time excitation force profile along with the PTO force signal from LTB's loadcells. The output displacement of WEC is commanded to LTB's Programmable Logic Controller (PLC) through Speedgoat's analog channel, and WEC's displacement gets translated into the vertical displacement of LTB's cart. NMPC, as the higher-level controller, receives the augmented state vector and the physical measurement of the PMSG's PTO force and computes the next PTO force command. The PTO force control block in Figure 4-7 scaling the PTO force command to q-axis current reference and implements the Field-Oriented Control (FOC) as the

low-level control to track the q-axis current command and generated the PWM signals through Speedgoat's PWM channels to drive the power converter.

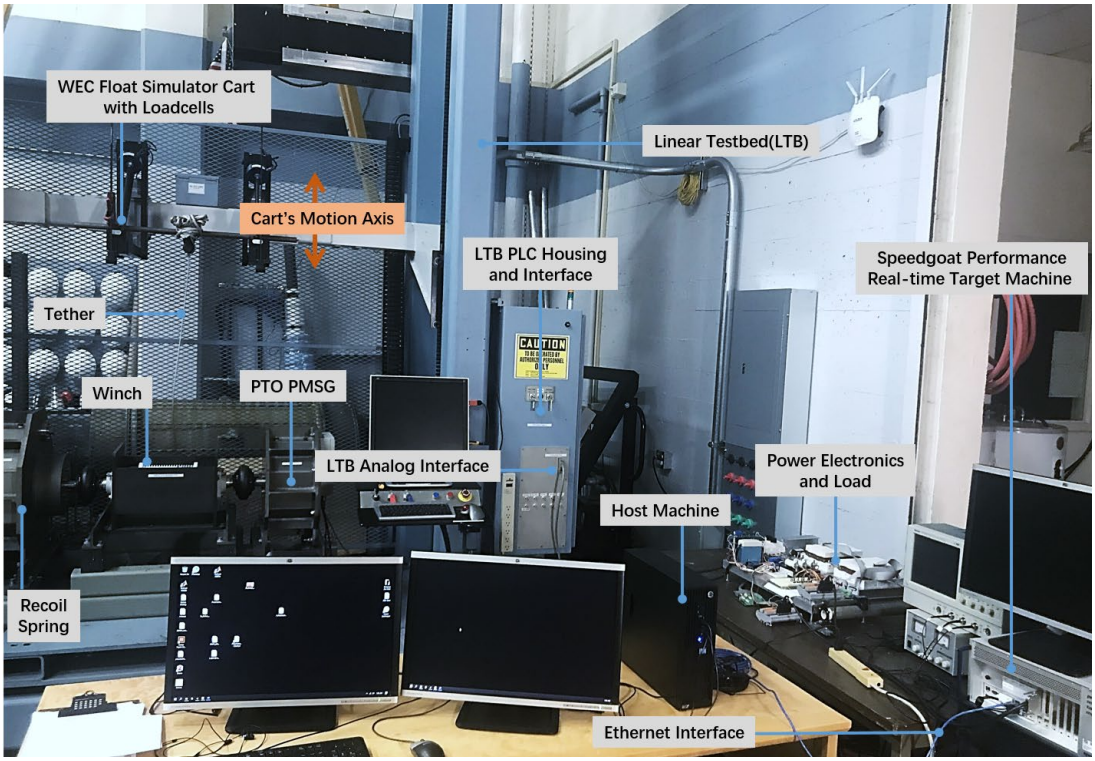

Figure 4-5 Experimental Setup for the hybrid testing platform.

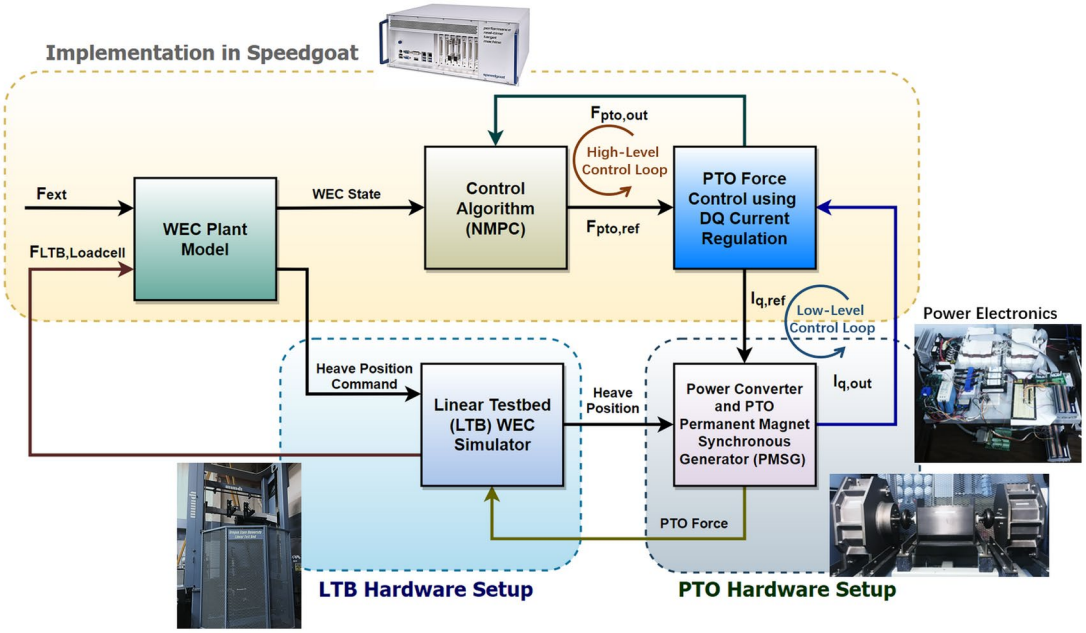

Figure 4-6 Block diagram for the hybrid testing scheme.

The data acquisition and signal processing block in Figure 4-7 reads various sensors and instruments and performs filtering and signal conditioning. It also implements Phase-locked-Loop (PLL) on the three-phase current measurements and performs Park transformation to compute the dq0-currents.

4.6 Experimental Results and Discussion

The excitation force profile for the hybrid testing is shown in Figure 4-8, which corresponds to an example sea state specified in Table 4-4. A step time of 0.1 sec is used for NMPC formulation, close to one-tenth of the peak wave period, while a faster sampling time of 0.001 sec is selected for the PTO current control loop. The corresponding experimental WEC PTO-velocity and displacement are plotted in Figure 4-9. The three-phase voltage and current outputs of the PMSG-PTO are shown in Figure 4-10 and Figure 4-11. The PTO force commanded by NMPC and the corresponding output PTO force of PMSG are shown on the same plot in Figure 4-112 and Figure 4-13. Two cases are considered to demonstrate the performance of the hybrid control setup: Unconstraint (UC) PTO force and Constrained (C) PTO force, $\left|F_{pto}\right| \leq 300\ N$, shown in Figure 4-12 and Figure 4-13, respectively. In either case, the output PTO force of PMSG successfully tracks the NMPC reference PTO force command. The plots of the dq0-currents are shown in Figure 4-14 for constraint and unconstraint PTO-force cases. Since the tracking of NMPC's PTO force command is achieved through a low-level FOC algorithm for the q-axis current regulation, Figure 4-15 shows the normalized plots of the q-axis currents and the corresponding PTO-force output from PMSG for constraint and unconstraint PTO-force cases, which shows the successful performance of the low-level control in terms of controlling the PTO

output force using the q-axis current of PMSG. The plots for the PTO power capture for the constraint and unconstraint PTO-force cases are shown in Figure 4-16. The PTO power capture's Exponentially Weighted Moving Average (EWMA) is also plotted in Figure 4-16. The experimental results show a successful performance of the proposed hybrids set up to test ocean wave energy systems.

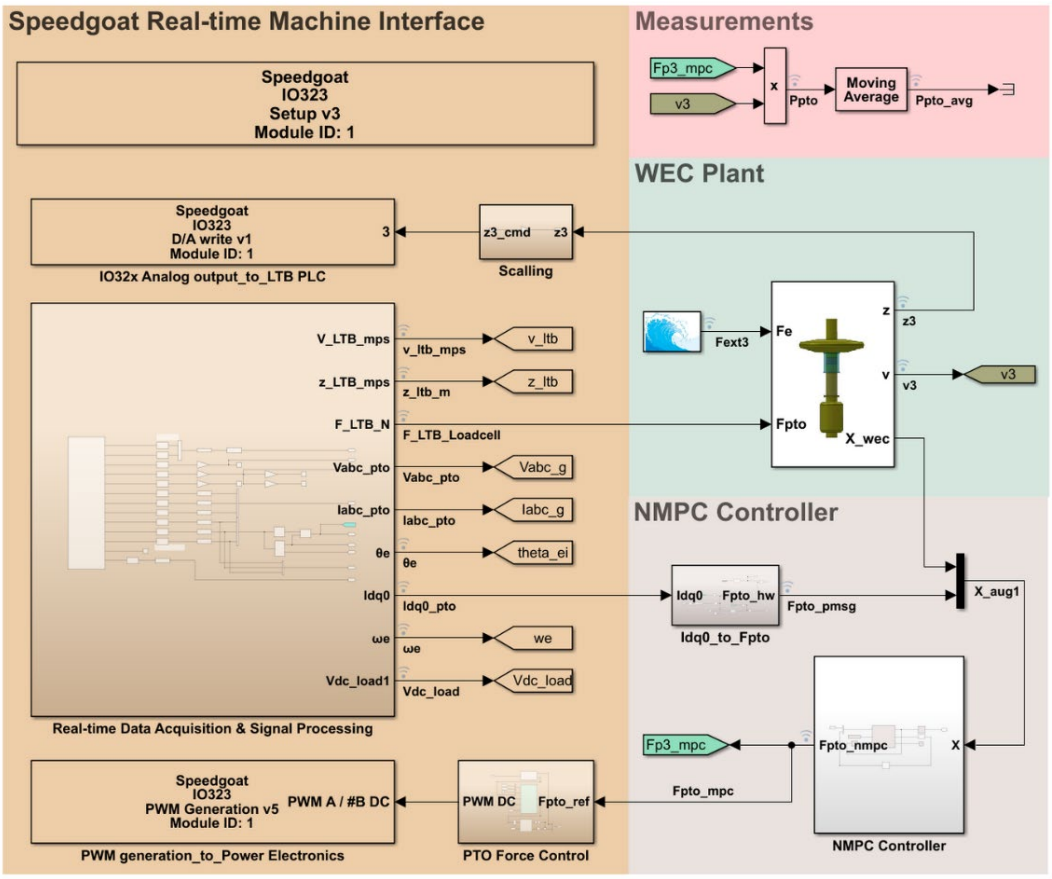

Figure 4-7 Simulink model for the code generation and deployment in the Speedgoat target machine for hybrid testing.

Table 4-4 Sea states for the experiment.

Parameter	Value
Significant Wave Height [m]	0.5
Peak Period [s]	8
Wave Spectrum Type	JONSWAP (JS)
Wave Class	Irregular

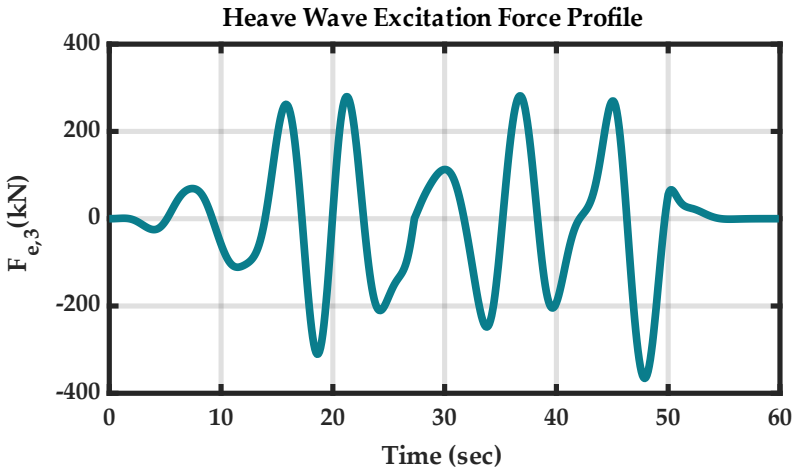

Figure 4-8 Real-time hybrid experimental results; Test profile of the wave excitation force.

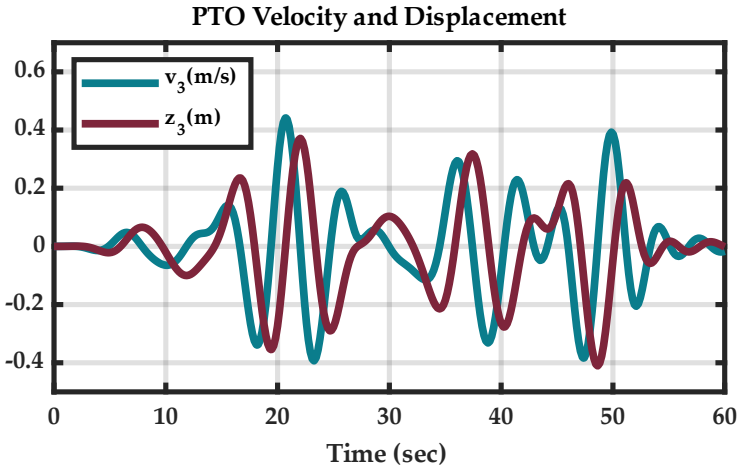

Figure 4-9 Real-time hybrid experimental results; PTO velocity and displacement.

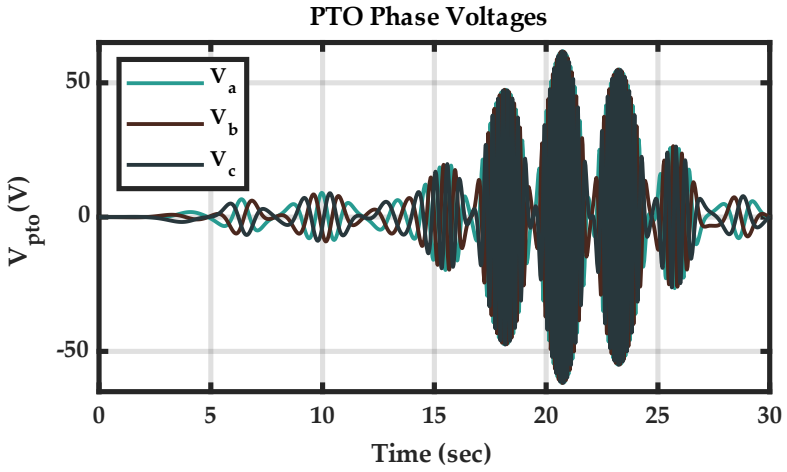

Figure 4-10 PMSG PTO generator outputs; Three-phase voltage outputs from the PMSG PTO stator.

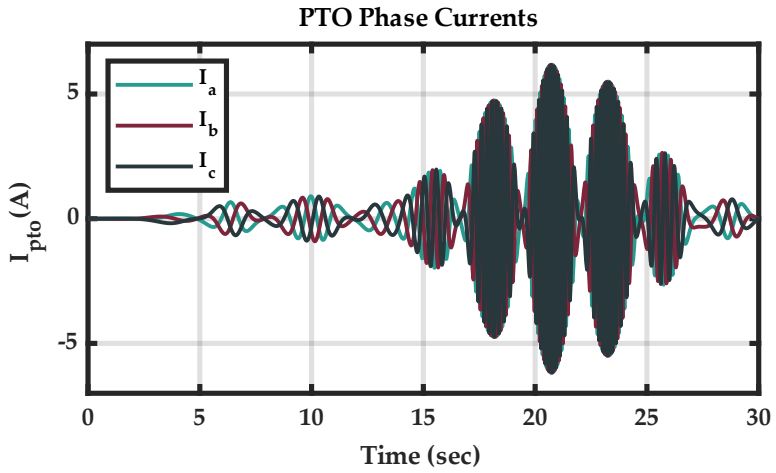

Figure 4-11 PMSG PTO generator outputs; Three-phase current outputs from the PMSG PTO stator.

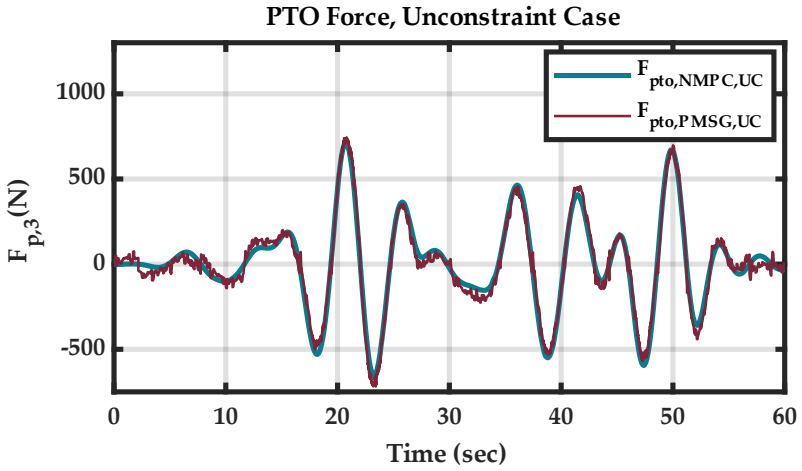

Figure 4-12 NMPC PTO Force and PMSG PTO force; Unconstraint PTO force.

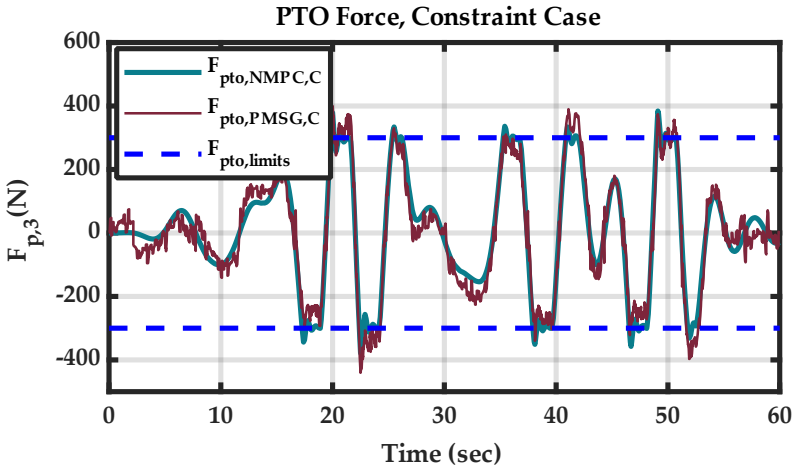

Figure 4-13 PTO Force command value by NMPC and corresponding PTO force output from the PMSG PTO: Constraint PTO force.

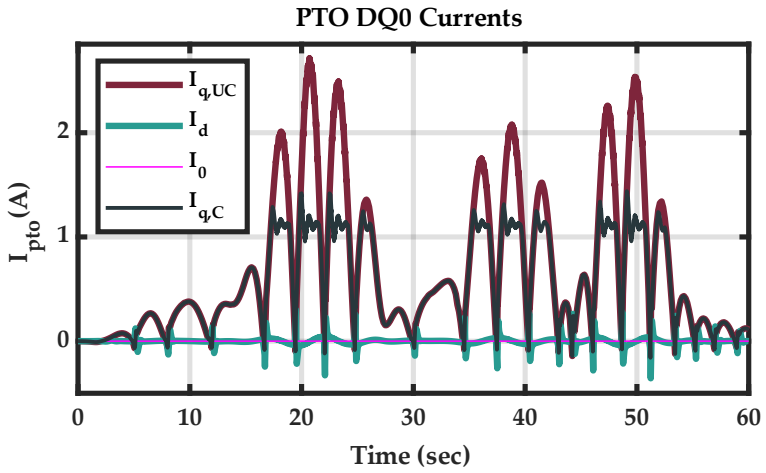

Figure 4-14 The dq0-current results with constraint and unconstraint PTO Force; PTO dq0-current outputs.

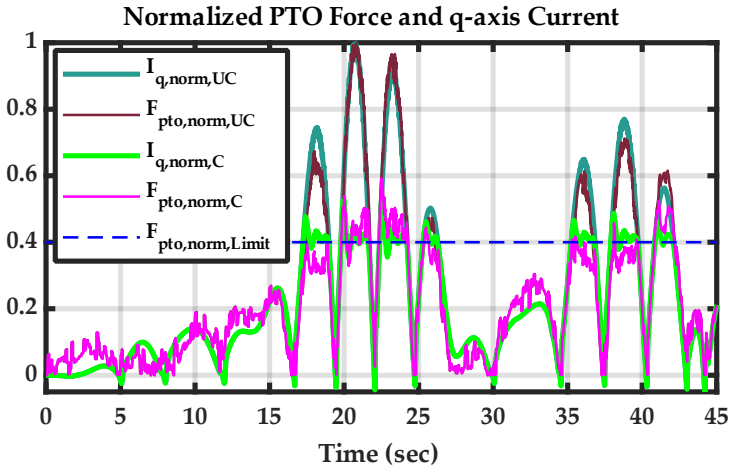

Figure 4-15 The dq0-current results with constraint and unconstraint PTO Force; Normalized PMSG-PTO force and q-axis current.

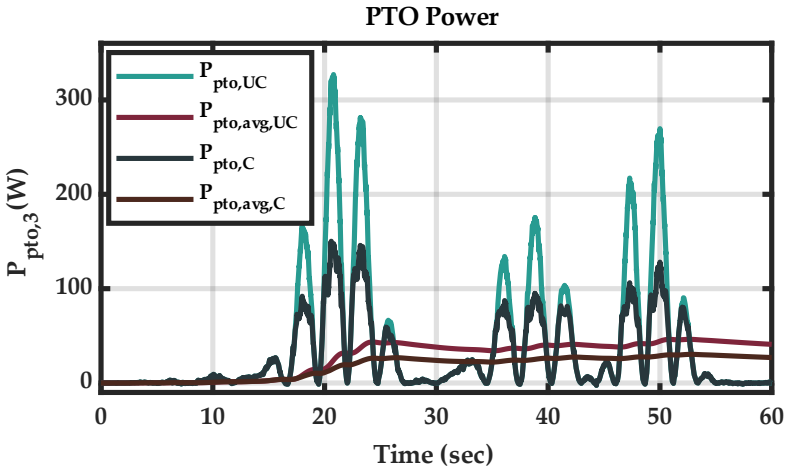

Figure 4-16 PTO power output; instantaneous and exponentially weighted moving average.

4.7 Conclusions

This article presents an experimental study on developing a hybrid testing platform for wave energy systems at the Wallace Energy System and Renewables Facility (WESRF) at Oregon State University. The hybrid testing strategy was implemented by dividing the system into virtual and physical components. The physical components involved a Permanent Magnet Synchronous Generator (PMSG) PTO generator coupled to a torsional restoring spring, ocean wave emulation Linear Testbed (LTB), power electronic converter, and sensors and instrumentation. The virtual part includes a numerical model of a point absorber WEC, the NMPC control algorithm, Field Oriented Control (FOC) of the power converter, and signal processing. A single degree of freedom WEC model of a single pod from the full-scale version of the Dehlsen Associates, LLC multi-pod CENTIPOD is modeled and simulated in real-time, and NMPC is designed to maximize the electrical output power of a hardware PTO mechanism. NMPC acts as the high-level controller, and its commanded PTO force is translated into a reference q-axis current of the PMSG-PTO generator through a faster low-level FOC. The full integrated testing of the hybrid scheme is performed using Speedgoat real-time performance machine interfaced with the hardware setup. The experimental results are presented, concluding with the successful performance of the proposed hybrid testing scheme. This setup can be used to experiment with advanced control algorithms for various heaving PTO mechanisms subjected to various sea states and advanced control algorithms.

4.8 References

1. Muetze, A.; Vining, J.G. Ocean Wave Energy Conversion - A Survey. In Proceedings of the Conference Record of the 2006 IEEE Industry Applications Conference Forty-First IAS Annual Meeting; October 2006; Vol. 3, pp. 1410–1417.
2. Ringwood, J.V. Wave Energy Control: Status and Perspectives 2020 □□This Paper Is Based upon Work Supported by Science Foundation Ireland under Grant No. 13/IA/1886 and Grant No. 12/RC/2302 for the Marine Renewable Ireland (MaREI) Centre. *IFAC-PapersOnLine* **2020**, *53*, 12271–12282, doi:10.1016/j.ifacol.2020.12.1162.
3. Brekken, T.K.A.; von Jouanne, A.; Han, H.Y. Ocean Wave Energy Overview and Research at Oregon State University. In Proceedings of the 2009 IEEE Power Electronics and Machines in Wind Applications; June 2009; pp. 1–7.
4. Leijon, M.; Waters, R.; Rahm, M.; Svensson, O.; Bostrom, C.; Stromstedt, E.; Engstrom, J.; Tyrberg, S.; Savin, A.; Gravrakmo, H.; et al. Catch the Wave to Electricity. *IEEE Power and Energy Magazine* **2009**, *7*, 50–54, doi:10.1109/MPE.2008.930658.
5. Hals, J.; Bjarte-Larsson, T.; Falnes, J. Optimum Reactive Control and Control by Latching of a Wave-Absorbing Semisubmerged Heaving Sphere. In Proceedings of the OMAE2002; 21st International Conference on Offshore Mechanics and Arctic Engineering, Volume 4, June 23 2002; pp. 415–423.
6. Garg, D.; Hager, W.W.; Rao, A.V. Pseudospectral Methods for Solving Infinite-Horizon Optimal Control Problems. *Automatica* **2011**, *47*, 829–837, doi:10.1016/j.automatica.2011.01.085.
7. Genest, R.; Ringwood, J.V. Receding Horizon Pseudospectral Control for Energy Maximization With Application to Wave Energy Devices. *IEEE Transactions on Control Systems Technology* **2017**, *25*, 29–38, doi:10.1109/TCST.2016.2554524.
8. Ringwood, J.V.; Bacelli, G.; Fusco, F. Control, Forecasting and Optimisation for Wave Energy Conversion. *IFAC Proceedings Volumes* **2014**, *47*, 7678–7689, doi:10.3182/20140824-6-ZA-1003.00517.
9. Richter, M.; Magana, M.E.; Sawodny, O.; Brekken, T.K.A. Nonlinear Model Predictive Control of a Point Absorber Wave Energy Converter. *IEEE Transactions on Sustainable Energy* **2013**, *4*, 118–126, doi:10.1109/TSTE.2012.2202929.
10. Faedo, N.; Olaya, S.; Ringwood, J.V. Optimal Control, MPC and MPC-like Algorithms for Wave Energy Systems: An Overview. *IFAC Journal of Systems and Control* **2017**, *1*, 37–56, doi:10.1016/j.ifacsc.2017.07.001.
11. Brekken, T.K.A. On Model Predictive Control for a Point Absorber Wave Energy Converter. In Proceedings of the 2011 IEEE Trondheim PowerTech; June 2011; pp. 1–8.
12. Genest, R.; Ringwood, J.V. A Critical Comparison of Model-Predictive and Pseudospectral Control for Wave Energy Devices. *J. Ocean Eng. Mar. Energy* **2016**, *2*, 485–499, doi:10.1007/s40722-016-0058-2.
13. Jia, Y.; Meng, K.; Dong, L.; Liu, T.; Sun, C.; Dong, Z.Y. Economic Model Predictive Control of a Point Absorber Wave Energy Converter. *IEEE Transactions on Sustainable Energy* **2021**, *12*, 578–586, doi:10.1109/TSTE.2020.3012755.

14. Rawlings, J.B.; Angeli, D.; Bates, C.N. Fundamentals of Economic Model Predictive Control. In Proceedings of the 2012 IEEE 51st IEEE Conference on Decision and Control (CDC); December 2012; pp. 3851–3861.
15. Li, G. Nonlinear Model Predictive Control of a Wave Energy Converter Based on Differential Flatness Parameterisation. *International Journal of Control* **2017**, *90*, 68–77, doi:10.1080/00207179.2015.1088173.
16. Haider, A.S.; Brekken, T.K.A.; McCall, A. Application of Real-Time Nonlinear Model Predictive Control for Wave Energy Conversion. *IET Renewable Power Generation n/a*, doi:10.1049/rpg2.12257.
17. Tedeschi, E.; Carraro, M.; Molinas, M.; Mattavelli, P. Effect of Control Strategies and Power Take-Off Efficiency on the Power Capture From Sea Waves. *IEEE Transactions on Energy Conversion* **2011**, *26*, 1088–1098, doi:10.1109/TEC.2011.2164798.
18. Bacelli, G.; Genest, R.; Ringwood, J.V. Nonlinear Control of Flap-Type Wave Energy Converter with a Non-Ideal Power Take-off System. *Annual Reviews in Control* **2015**, *40*, 116–126, doi:10.1016/j.arcontrol.2015.09.006.
19. Falcão, A.F.O.; Henriques, J.C.C. Effect of Non-Ideal Power Take-off Efficiency on Performance of Single- and Two-Body Reactively Controlled Wave Energy Converters. *J. Ocean Eng. Mar. Energy* **2015**, *1*, 273–286, doi:10.1007/s40722-015-0023-5.
20. Haider, A.S.; Brekken, T.K.A.; McCall, A. Real-Time Nonlinear Model Predictive Controller for Multiple Degrees of Freedom Wave Energy Converters with Non-Ideal Power Take-Off. *Journal of Marine Science and Engineering* **2021**, *9*, 890, doi:10.3390/jmse9080890.
21. The Future of Testing Wave Energy Technology. *Innovation News Network* 2021.
22. Bachynski, E.E.; Chabaud, V.; Sauder, T. Real-Time Hybrid Model Testing of Floating Wind Turbines: Sensitivity to Limited Actuation. *Energy Procedia* **2015**, *80*, 2–12, doi:10.1016/j.egypro.2015.11.400.
23. Home Available online: https://www.validhtp.eu (accessed on 23 August 2021).
24. Peng, W.; Zhang, Y.; Yang, X.; Zhang, J.; He, R.; Liu, Y.; Chen, R. Hydrodynamic Performance of a Hybrid System Combining a Fixed Breakwater and a Wave Energy Converter: An Experimental Study. *Energies* **2020**, *13*, 5740, doi:10.3390/en13215740.
25. Wallace Energy Systems & Renewables Facility | | Oregon State University Available online: https://wesrf.engr.oregonstate.edu/ (accessed on 23 August 2021).
26. van Rij, J.; Yu, Y.-H.; McCall, A.; Coe, R.G. Extreme Load Computational Fluid Dynamics Analysis and Verification for a Multibody Wave Energy Converter.; American Society of Mechanical Engineers Digital Collection, November 11 2019.
27. Ecomerit Technologies Available online: http://www.ecomerittech.com/centipod.php (accessed on 14 August 2021).
28. WEC-Sim (Wave Energy Converter SIMulator) — WEC-Sim Documentation Available online: https://wec-sim.github.io/WEC-Sim/ (accessed on 27 March 2021).
29. Wamit, Inc. - The State of the Art in Wave Interaction Analysis Available online: https://www.wamit.com/ (accessed on 28 March 2021).

30. Busca, C.; Stan, A.-I.; Stanciu, T.; Stroe, D.I. Control of Permanent Magnet Synchronous Generator for Large Wind Turbines. In Proceedings of the 2010 IEEE International Symposium on Industrial Electronics; July 2010; pp. 3871–3876.
31. Custom Machines | Automated Laser Workstations | Mundt Available online: http://www.mundtinc.com/products/custom/ (accessed on 23 August 2021).
32. SKiiP 603 GD123-3DUL V3 | SEMIKRON Available online: https://www.semikron.com/products/product-classes/ipm/detail/skiip-603-gd123-3dul-v3-20452028.html (accessed on 23 August 2021).

5 General Conclusions

This work presented the application of Nonlinear Model Predictive Control (NMPC) for ocean wave energy conversion systems. The research has been focused on a class of Wave Energy Converters (WEC) problems in which the cost functional is not in a standard quadratic form, and the WEC model includes the nonlinear hydrodynamic effects, such as the fluid viscous drag. The proposed technique's applications are presented to maximize the energy produced by a Wave Energy Converter (WEC) when the cost index is a piecewise discontinuous functional of system variables. The presented framework is based on pseudo-quadratization and weight scheduling, implemented using the ACADO toolkit and the MPC toolbox in MATLAB/Simulink. The proposed strategy features code generation and deployment on the real-time target machines for industrial applications. The proposed methodology successfully maintained an overall feasible operation of the real-time NMPC problem in simulation as indicated by the status port of the NMPC QP-solver. The experimental implementation on the Speedgoat target machine confirmed the optimal power capture results from the simulation.

The NMPC formulation is extended for MIMO waver energy conversion systems, and real-time implementation of NMPC was presented for a nonlinear 2-DoF WEC based on Dehlsen Associates' CENTIPOD multi-pod WEC device, with non-ideal PTOs in the heave and pitch axes. The three pods of the WEC device are assumed identical, and a nonlinear state-space model of a single pod is developed. An NMPC controller is implemented for a 2-DoF WEC device with the cost functional based on a case study PTO model with a highly nonlinear PTO current-force characteristic. The

results of the linear MPC are compared with NMPC for the sea states of interest (irregular waves with Pierson Moskowitz spectrum) under linear and nonlinear hydrodynamic conditions in WEC-Sim. An average of 35% processor load was observed per sampling interval during testing. An overall 5% increase in total power output by a single pod is obtained by NMPC compared to linear MPC under linear hydrodynamic conditions and 10.6% under nonlinear hydrodynamic conditions.A 35% increase in net output power is obtained by the 2-DoF WEC device compared to the 1-DoF heave only, and a 129% increase compared to the 1-DoF pitch only. While the result reflects only a single sea state, the improvement is likely to be reflected similarly in annual energy production (AEP). The AEP would have a substantive impact on the Levelized Cost of Energy (LCOE). The present work did not consider the cross-coupling between the three pods of the CENTIPOD device.

Lastly, an experimental study was presented on developing a hybrid testing platform for wave energy systems at the Wallace Energy System and Renewables Facility (WESRF) at Oregon State University. The hybrid testing strategy was implemented by dividing the system into virtual and physical components. The physical components involved a Permanent Magnet Synchronous Generator (PMSG) PTO generator coupled to a torsional restoring spring, ocean wave emulation Linear Testbed (LTB), power electronic converter, and sensors and instrumentation. The virtual part includes a numerical model of a point absorber WEC, the NMPC control algorithm, Field Oriented Control (FOC) of the power converter, and signal processing. A single degree of freedom WEC model of a single pod from the full-scale version of the Dehlsen Associates, LLC multi-pod CENTIPOD is modeled and simulated in real-time, and

NMPC is designed to maximize the electrical output power of a hardware PTO mechanism. NMPC acts as the high-level controller, and its commanded PTO force is translated into a reference q-axis current of the PMSG-PTO generator through a faster low-level FOC. The full integrated testing of the hybrid scheme is performed using Speedgoat real-time performance machine interfaced with the hardware setup. The experimental results are presented, concluding with the successful performance of the proposed hybrid testing scheme. This setup can be used to experiment with advanced control algorithms for various heaving PTO mechanisms subjected to various sea states and advanced control algorithms.